Dalton Transactions

ROYAL SOCIETY OF CHEMISTRY

PAPER

View Article Online
View Journal | View Issue

Cite this: *Dalton Trans.*, 2025, **54**, 12259

Fluorescent chemosensing of epinephrine by a bis-boronic molecular receptor in aqueous media: crystal structure, spectroscopic studies and visual detection†

Alejandro O. Viviano-Posadas, [a] Josue Valdes-García, *[a] María K. Salomón-Flores, [a] Diego Martínez-Otero, [b] Joanatan M. Bautista-Renedo, [b] Nelly González-Rivas, [b] Hilda Sánchez-Vidal,[c] Juan M. German-Acacio, [c] Jesús Valdés-Martínez [a] and Alejandro Dorazco-González *[a]

Selective recognition and sensing of neurotransmitters in aqueous media using artificial receptors is an attractive but challenging goal in modern supramolecular chemistry. Despite advances in the development of optical receptors for some neurotransmitters, such as dopamine, limited efforts have been invested in developing receptors for epinephrine, a neurotransmitter of paramount importance and a widely used drug for heart attacks. Herein, a new fluorescent molecular receptor (referred to as **1**) based on a 1,3-bis-benzimidazole-benzene derivative covalently linked to two phenyl boronic acids was synthesized, structurally characterized *via* single-crystal X-ray diffraction, and studied in-depth as a receptor for four catecholamine-based neurotransmitters as well as several nucleosides, monosaccharides and L-tyrosine in water at physiological pH. Receptor **1** is hydrostable and exhibits fluorescence emission at 408 nm, originated from intraligand (IL) [π–π^*] transitions, as supported by TD-DFT calculations. The addition of epinephrine/norepinephrine at micromolar concentrations to an aqueous solution of **1** induces significant and rapid fluorescence changes, whereas in the presence of dopamine, L-DOPA, adenosine, guanosine, glucose, fructose, galactose, ribose and L-Tyr, only modest optical changes are observed. Bis-boronic receptor **1** was found to exhibit high affinity for epinephrine (K = 1.29 × 10^5 M^{-1}), with good selectivity over other closely related neurotransmitters, including dopamine and L-DOPA. The affinity of epinephrine for **1** is an order of magnitude greater than that for norepinephrine. Such epinephrine affinity/selectivity for a molecular receptor is still rare. Spectroscopic techniques (fluorescence, ^{11}B NMR, fluorescence lifetimes), mass spectrometry, single-crystal X-ray diffraction, DFT calculations and atoms in molecules analysis revealed that epinephrine binds to **1** in a 1 : 2 (receptor : analyte) stoichiometry. This two-point recognition involves sp^3 boronate–catechol condensation and multiple hydrogen bonds (OH···N and NH···N) between the aliphatic chain of epinephrine and the imidazole ring of **1**, along with intermolecular interactions between the two epinephrine molecules in the resulting supramolecular structure. The efficient fluorescent response of **1** to epinephrine can be utilized in quantitative sensing of this bioanalyte in real pharmaceutical samples. Furthermore, a chromogenic sensing ensemble comprising **1** and the commercial dye Alizarin Red S was developed, in which epinephrine can be visually detected *via* an indicator displacement assay through a color change at micromolar concentrations.

Received 1st April 2025,
Accepted 14th July 2025

DOI: 10.1039/d5dt00784d

rsc.li/dalton

[a]*Institute of Chemistry, National Autonomous University of Mexico, Ciudad Universitaria, México, 04510 CDMX, Mexico. E-mail: adg@unam.mx*
[b]*Centro Conjunto de Investigación en Química Sustentable, UAEM-UNAM, Carretera Toluca-Atlacomulco Km 14.5, C. P. 50200, Toluca, Estado de México, Mexico*
[c]*Red de Apoyo a la Investigación, Coordinación de la Investigación Científica-UNAM, Instituto Nacional de Ciencias Médicas y Nutrición SZ, Ciudad de México, CP 14000, Mexico*

†Electronic supplementary information (ESI) available: General information, X-ray crystallographic data, and crystal packing diagrams of **1** and **2**; ^{1}H, ^{13}C, ^{11}B NMR, IR-ATR, and MS spectra for **1** and **2**; spectroscopic experiments; HPLC-UV experiments and DFT calculations. CCDC Cambridge Crystallographic Data Centre under CCDC 2252384 and 2252385. For ESI and crystallographic data in CIF or other electronic format see DOI: https://doi.org/10.1039/d5dt00784d

Introduction

The selective optical sensing of neurotransmitters (NTs) derived from biogenic catecholamines, such as dopamine, L-DOPA, epinephrine (adrenaline), and norepinephrine (noradrenaline), by synthetic molecular receptors in aqueous environments remains an active area of research and ongoing challenge in supramolecular chemistry and analytical sciences.[1–6] These NTs are essential signaling molecules that direct neuronal network functions in humans, including motor control, memory, learning, feeding behavior and sensory perception.[7–9] Dopamine and epinephrine also function as hormones. In particular, epinephrine plays a critical role in physiological processes such as glycogenolysis, increased plasma lactate levels and enhanced forced production during rapid muscle contraction.[10–13] For this reason, epinephrine is prohibited in sports by the World Anti-doping Agency.

In general, NTs are present at *sub*-micromolar concentrations in the nervous system and biofluids,[14–16] making their molecular recognition and optical sensing a challenging task in terms of molecular design of the receptor and its functionality in aqueous media. For instance, dopamine exists in nanomolar concentrations in biofluids, with elevated levels linked to cardiotoxic effects.[17] In contrast, reduced dopamine levels have been associated with neurodegenerative diseases such as Alzheimer's and Parkinson's diseases.[18–21]

Epinephrine is considered one of the pivotal NTs because it regulates heart rate, blood pressure and memory functions.[22] This catecholamine is typically present at nanomolar concentrations (~5–58 nM) in human serum and urine,[4,23] and its level serves as a chemical indicator for conditions such as Parkinson's disease,[24] schizophrenia,[25] depression and heart failure.[26–29] Furthermore, epinephrine is widely used as a drug for cardiac resuscitation and the treatment of bronchial asthma.[30,31] Despite the evident need for selective and potent optical chemosensors for epinephrine, only a limited number of luminescent receptors have been reported to date, especially when compared with the abundance of optical molecular receptors developed for dopamine.[1,2,32–39] Currently, an overwhelming majority of epinephrine detection methods are based on electrochemical sensors,[23,25,40–42] biosensors involving enzymatic assays,[43–47] and luminescent/colorimetric nanomaterials such as carbon quantum dots (C-QDs),[27,48–50] AlSe,[51] CdTe,[52] Au-nanoclusters,[53,54] and ZnO-nanorods.[55] However, these sensor-based analytical methods still face some drawbacks for practical applications. In particular, biosensors and nanomaterial-based systems often require multistep fabrication, long analysis times (typically several minutes), and specialized laboratory facilities. Furthermore, most of these electrochemical (bio)sensors lack high selectivity because their detection mechanisms rely on the chemical or enzymatic oxidation of the catechol ring. As a result, interference from other NTs, L-tyrosine, and uric acid is commonly observed.[42,48,50,51]

Among the various techniques for NTs sensing, fluorescence is particularly desirable owing to its inherent high sensitivity, large signal-to-noise ratio and rapid analytical response.[3,37–39,56] In this context, the literature includes only a few examples of fluorescent molecular receptors capable of direct and specific sensing of epinephrine, such as cyanine-based dyes[57] and donor–acceptor Stenhouse dyes,[26] which exploit the nucleophilicity of the secondary amine group in epinephrine to generate fluorescent products, typically under non-aqueous conditions.

Alternatively, luminescent sensing of epinephrine in aqueous media has been achieved using phenylboronic acid (PBA) derivatives linked to fluorophores such as pyrene,[58] quinolone,[59] and alizarin complexone,[29] where the $-B(OH)_2$ group serves as a binding site for catechol. These receptors exhibit moderate binding affinities ($K \sim 200$–$36\,000\ M^{-1}$) and are thus suitable for sensing epinephrine in the micromolar concentration range, but not significantly lower levels.

Neutral sp^2-hybridized mono-boronic acids are known to bind with compounds bearing polyol groups, anions and or catechol units with high affinity through reversible anionic sp^3 boronate formation in aqueous media;[60–63] however, simple PBA exhibits relatively low affinity toward catechol at physiological pH (K = 830 M^{-1}).[64] Therefore, the development of more sophisticated receptors is essential to achieve improved binding affinity and selectivity for epinephrine. Previously, Schrader reported a selective receptor for epinephrine based on a *p*-xylylene macrocycle that operates through a combination of hydrogen bonding, electrostatic interactions and van der Waals forces. However, due to the receptor's high flexibility, its binding affinity was relatively low ($K \approx 10^2\ M^{-1}$) and it lacked fluorescent units.[65]

In principle, the creation of an efficient and selective receptor for epinephrine is achievable by designing a water-soluble fluorophore incorporating: (1) high-affinity binding sites for the catechol moiety, such as boronic acids and (2) hydrogen bond acceptor groups that specifically recognize the amine and hydroxyl groups of the aliphatic chain – features that represent the most significant structural differences compared to other NTs. To the best of our knowledge, luminescent bis-boronic acid–based receptors containing two cooperative binding sites that include hydrogen bond acceptors for epinephrine and related NTs have not been reported. Here, we summarize the results obtained for fluorescent bis-benzimidazole-benzene derivatives bearing two boronic acid groups including their synthesis, crystal structure, acid–base properties, spectroscopic sensing of neurotransmitters in aqueous media, epinephrine quantification in pharmaceutical samples, and DFT calculations.

Results and discussion

Synthesis, crystal structures and Hirshfeld surface analysis

For these investigations, the bis-boronic acid-based receptor **1** was successfully synthesized *via* the two-step synthetic route shown in Scheme 1. The intermediate L, a derivative of 1,3-bis-benzimidazole-benzene, was obtained by a cyclodehydration reaction between *o*-phenylenediamine and isophthalic acid in

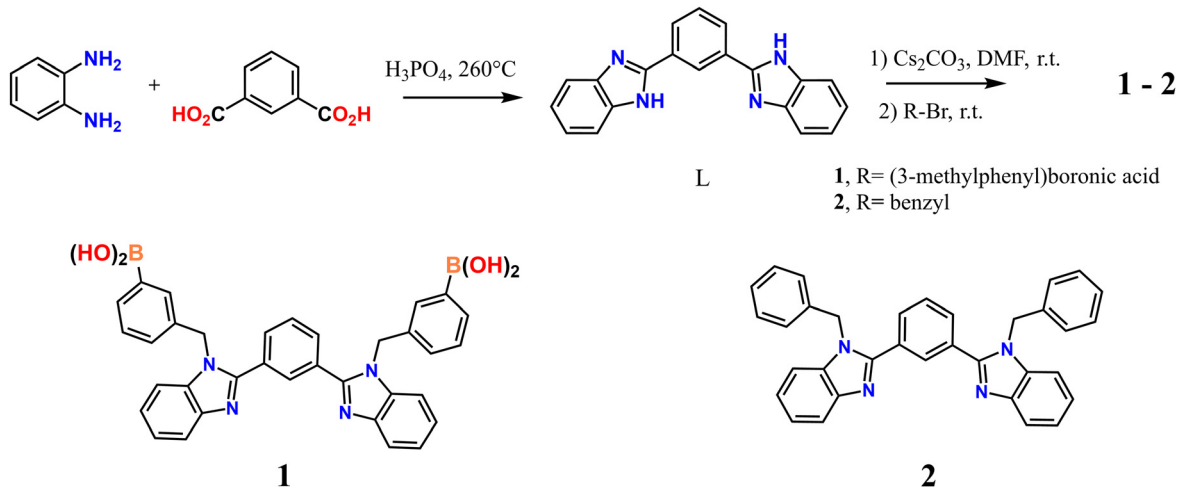

Scheme 1 General synthesis of receptors **1** and **2** employed in this work.

H_3PO_4.[66] Subsequent treatment of L with 3-(bromomethyl) phenylboronic acid in dry DMF under an N_2 atmosphere afforded the bis-boronic compound **1**, which was isolated in good yield. The purity and identity of **1** were confirmed by (^{1}H, ^{13}C, ^{11}B, and HSQC) NMR spectroscopy, ESI(–) mass spectrometry, IR-ATR (Fig. S1–S6†) and elemental analysis (C, H, and N). A reference compound **2**, lacking boronic acid groups, was synthesized using benzyl bromide instead of 3-(bromomethyl)phenylboronic acids. The identity of **2** was verified by ^{1}H and ^{13}C NMR, MS and IR-ATR (Fig. S7–S10†).

The ^{11}B NMR spectrum of **1** in CD_3OD displayed only a single signal at 29.91 ppm (Fig. S3†), which can be attributed to an sp^2-hybridized boronic acid.[67,68] In the ESI(–) mass spectrum of **1** recorded in DMSO–H_2O (v/v, 9 : 1), a charged species was observed at m/z = 673.2, corresponding to the monoboronate form of **1**, $\{$**1**-B(OH)$_3$ + DMSO$\}^-$ (where **1**-B(OH)$_3$ represents **1** with one sp^3-tetrahedral boronate anion), and the signal isotopically resolved; the multiplicity of the peaks, separated by 1.0 m/z unit, closely matches the theoretical distribution expected for a compound containing two B atoms (Fig. S5†).

Single crystals suitable for X-ray analysis were obtained for **1** and **2** by slow evaporation at r.t. from THF-H_2O (1 : 1, v/v) and methanolic solutions, respectively (see Tables S1–S3 in ESI† for crystallographic data, hydrogen bond parameters within the crystal packing and selected distances/angles around B atoms in **1**). Fig. 1 shows perspective molecular views of **1** and **2**. In the crystal structure of **1**, both B atoms adopt sp^2 hybridization with ideal trigonal planar geometry ($\sum\sphericalangle$(X–B–X) = 359.9–360.0°) and are separated by a B···B distance of 11.639(7) Å; this relatively large separation between boronic acid groups suggests that they may function as independent recognition sites for catechol rings rather than as cooperative, chelating binding sites.[69] The correlation between the crystal structure and ^{11}B NMR spectrum supports the sp^2 hybridization of the B atoms. Favorably for pre-organization, both boronic acid groups are positioned on the same side of the receptor plane, adopting a *syn–syn* type conformation with respect to the 1,3-bis(benzimidazol-2-yl)benzene fragment. The rings of the bis(benzimidazol-2-yl)benzene core are non-coplanar; the dihedral angles between the central phenylene plane and the two benzimidazole rings are 27.86° and 50.41°, respectively.

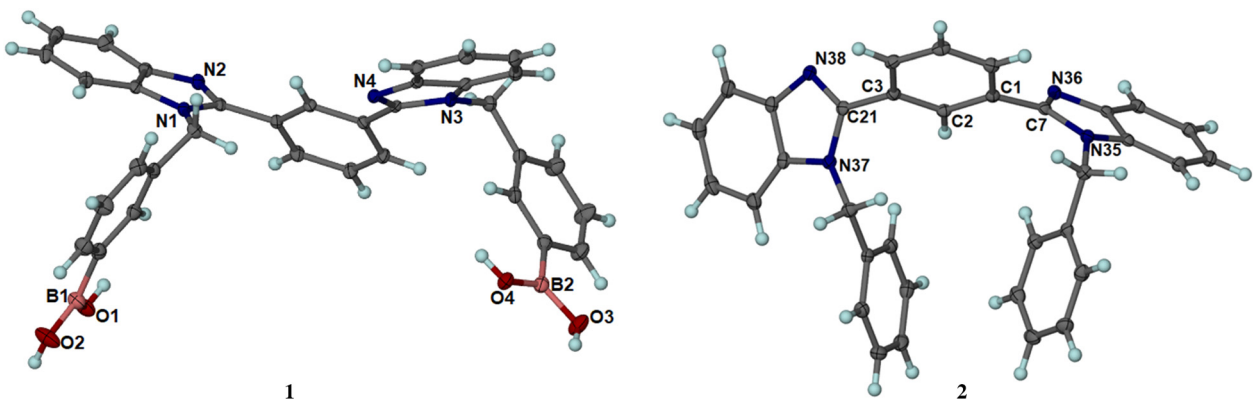

Fig. 1 ORTEP diagrams of **1** and **2** at 50% of probability. THF solvent molecules in the structure of **1** have been omitted for clarity.

Structural analysis of **1** shows that the crystal lattice contains three THF molecules, one of which is positioned near a $-B(OH)_2$ group, forming a H-bond of the type B(2)–O(3)–H(30)$\cdots$O(5)$_{THF}$ (Fig. S11†).

Fig. 1also presents a molecular view of **2**, which crystallizes in the chiral space group $P2_12_12_1$, despite being a non-chiral molecule. Similar cases of supramolecular chirality have been reported for 2-propyl-1*H*-benzimidazole.[70]

This solid-state chirality can be attributed to the torsion angles of 58.14° and 126.87° for C(2)–C(3)–C(21)–N(37) and C(2)–C(1)–C(7)–N(35), respectively, between the central phenylene ring and the lateral benzimidazole rings. These torsions result in a two-winged, propeller-like conformation, with considerable twisting of the benzimidazole unit.

The pendant benzyl groups adopt a *syn–syn* conformation relative to the plane of the central phenylene ring. Along each crystallographic axis, two 2-fold screw axes are present, leading to the stacking columnar and helical arrangements of the molecules (Fig. S12†).

The supramolecular arrangement within the crystal of **1** is stabilized by diverse intermolecular interactions, including type B–O–H$\cdots$N$_{imidazole}$ and B–O–H$\cdots$O–B hydrogen bonds as well as π–π stacking as revealed by Hirshfeld surface (HS) analysis[71] and two-dimensional fingerprint plots[72] (Fig. S13†). Fig. 2A highlights the overall molecular arrangement along the *a*-axis, emphasizing the interplay between H-bonds of the type B(2)–OH$\cdots$N(4)$_{imidazol}$ and π–π interactions between imidazole rings. Fig. 2B clearly depicts the formation of one-dimensional chains *via* B(1)–O–H$\cdots$O–B(1) hydrogen bonds (Table S2†), which involve a typical dimeric $R_2^2(8)$ homo-synthon characteristic of phenylboronic acids.[73] In this homo-synthon, the hydroxyl groups adopt a common *syn–anti* conformation. Fig. 2C illustrates the two types of hydrogen bonds on the Hirshfeld surface mapped with the d_{norm} parameter of **1**, while Fig. 2D and Table S4† confirm the presence of π–π interactions, as indicated by the shape index property of the Hirshfeld surface.

In contrast, the Hirshfeld surface analysis and two-dimensional fingerprint plots of **2** indicate that there are no significant π–π stacking interactions. In this case, molecular packing stability arises predominantly from weak C–H$\cdots$π and C–H$\cdots$N interactions, as shown in Fig. S13 and Table S5.†

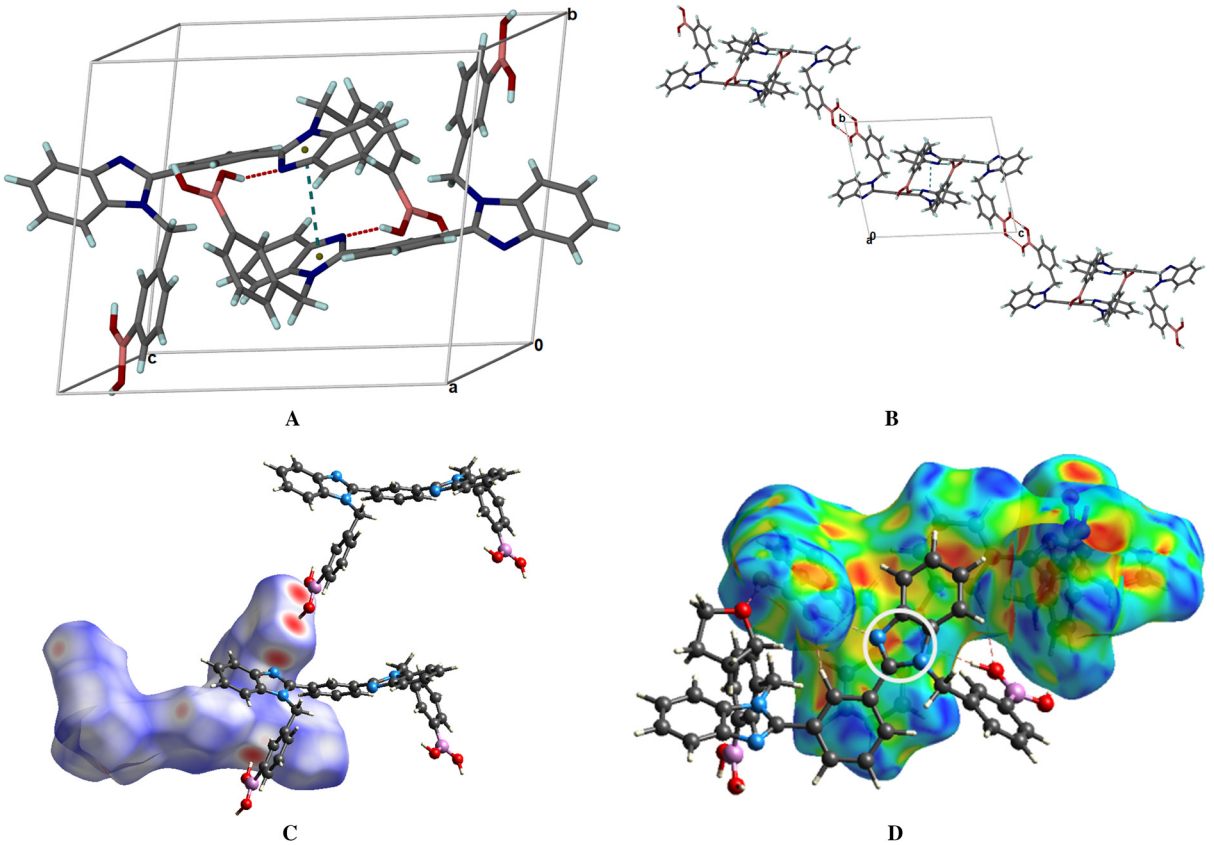

Fig. 2 (A) Crystal packing viewed along the *a*-axis, illustrating the overall molecular arrangement with H-bonds, B(2)–O–H$\cdots$N$_{imidazole}$ (red dashed lines) and π–π stacking interactions (green dashed lines). The π–π distance (3.9332(8) Å) was measured between the planes of the benzimidazole rings. (B) Crystal packing viewed along the *c*-axis, highlighting the 1D H-bond chains induced by $R_2^2(8)$ homo-synthon between B(1)–(OH)$_2$ groups. (C) Hirshfeld surface mapped with d_{norm}, illustrating H-bonds. (D) Hirshfeld surface mapped with the shape index; the white circle indicates the π–π stacking interaction between imidazole rings.

Optical and acid–base properties

Compounds **1** and **2** are soluble in buffered water (10 mM MOPS, pH = 7.4) up to 40 μM, which is sufficient for UV-Vis and fluorescence spectroscopic sensing studies; however, in water, titration experiments were poorly reproducible due to a decrease in solubility in the presence of NTs. The addition of 10 vol% of CH_3OH enabled stable solutions of **1** and **2** to be maintained in the presence of NTs over extended periods; thus, this solvent mixture was used for all subsequent spectroscopic studies.

The absorption and emission maxima of **1** and **2** (10 μM) in pure water at pH 7.40 are summarized in Table S6.† Both compounds exhibit an intense absorption band in the range of 250–340 nm (Fig. S14†), which is typically attributed to intraligand (IL) [π–π*] electronic transitions of the benzimidazole moieties.[74]

To better understand the absorption spectrum of **1**, time-dependent density functional theory (TD-DFT) calculations were performed using its crystal structure as the ground-state geometry.

Main transitions are summarized in Table S7,† along with their wavelengths, oscillator strengths, and orbital assignments. Analysis of natural transition orbitals (NTOs) indicates that singlet transitions above 270 nm exhibit spin-allowed intraligand (IL) [π–π*] character, centered on the bis(benzimidazol-2′-yl)benzene fragment. In addition, a differential potential energy surface was calculated for the lowest-energy absorption by subtracting the S_1 (first excited state) at S_0 (ground state). The surface shows a decrease in electronic density on the benzimidazole moiety and an increase on the benzene fragment (Fig. S15†). Low-energy blue emission bands of **1** and **2** at ~408 nm (λ_{ex} = 290 nm) are commonly attributed to ^{1}ILCT π–π* transitions from the excited states of bis(benzimidazol-2′-yl)benzene.[74]

On the other hand, it is well known that there is a correlation between the pK_a values of boronic acids and their ability to bind diols/catechols.[75] Therefore, prior to exploring the binding affinity of **1** and NTs, the pK_a values of **1** were estimated by fluorescence spectroscopy.

Receptor **1** possesses four ionogenic groups: two imidazole rings and two equivalent PBA groups. For this compound, three pK_a values were accurately determined from a fluorescence pH titration experiment; pK_a = 4.93 ± 0.12, pK_a = 5.81 ± 0.07 and pK_a = 7.97 ± 0.03 (see Fig. S16†). Some related benzimidazole molecules exhibit pK_a values between 4.82 and 6.83 based on UV-Vis pH profiles,[76] and for bis-benzo[*d*]imidazole derivatives, pK_a values ranging from 3.74 and 6.71 have been reported.[77]

Fig. S17A† shows the results of a UV-Vis pH titration experiment of **1** (10 μM), from which three pK_a values were calculated: pK_a = 5.05 ± 0.06, pK_a = 5.70 ± 0.16, and pK_a = 7.99 ± 0.04. The spectrophotometric titration profile at 294 nm is illustrated in Fig. S17B.† These three pK_a values are practically the same to those estimated by fluorescence, indicating that the calculated acid-base constants obtained by both techniques correspond to the ground state.

Previous reports on boronic acids with similar acid–base constants, estimated by UV-Vis and fluorescence, are also primarily attributed to the ground state, with negligible contributions from the excited state.[60–63]

It may be inferred that the first two pK_a values below 7.0 correspond to the two consecutive deprotonation steps of the benzimidazole rings; however, the assignation of these pK_a values, particularly for the boronic acid moieties, remains unclear.

An attempt to identify the acid–base dissociation of the $-B(OH)_2$ groups by ^{11}B NMR titrations was unsuccessful owing to the insufficient solubility of **1** in pure D_2O required for these measurements. During diol binding, boronic acids become significantly more acidic, resulting in a decrease in their pK_a values.[78] Therefore, to identify the acid–base dissociation constants of the boronic groups, a fluorescence pH titration experiment was performed with receptor **1** (5.0 μM) in the presence of 100 mM D-glucose. Fig. 3A shows the set of emission spectra for the pH titration of **1** with glucose. Fluorimetric titration profiles of **1** in the absence and presence of glucose are shown in Fig. 3B. The fluorometric profile data at 408 nm for **1** in the presence of glucose also fits well with three pK_a values: pK_a = 4.84 ± 0.13, pK_a = 6.08 ± 0.08 and pK_a = 7.21 ± 0.05.

Overall, the addition of glucose shifts the pK_a value of 7.97 by approximately 0.8 units to a lower value (inset of Fig. 3B). This observation provides evidence that this pK_a corresponds to the two equivalent phenylboronic acid groups. In contrast, the two pK_a values below 7.0 remain practically constant, suggesting that they correspond to the consecutive deprotonation steps of the two benzimidazole rings.

The phenylboronic acid moieties in **1** are slightly more acidic than mono-boronic acid (PBA, pK_a ~ 8.7),[64] yet the observed decrease in pK_a value to 7.21 in the presence of glucose is significant because it suggests that the $-B(OH)_2$ groups can be converted into their anionic tetrahedral diol-binding forms at a pH close to the physiological value of 7.4. It is well known that complex formation between boronic acids and diols occurs only at pH ≥ pK_a of the corresponding tetrahedral boronate species.[64] Given that the catechol moiety binds more strongly to boronic acids than polyols such as glucose, receptor **1** should be suitable for the fluorescent sensing of catecholamines at pH = 7.4.

Fluorescence sensing of NTs

Aqueous solutions of **1** containing 10 vol% of CH_3OH at micromolar concentrations remain photostable for several days. Taking advantage of the strong blue emission of **1**, a relative selectivity experiment was performed to evaluate receptor **1** towards NTs and other biologically relevant polyols (nucleosides and monosaccharides). For this experiment, dopamine, epinephrine, norepinephrine, L-DOPA, adenosine, guanosine, glucose, fructose, galactose and ribose and catechol ($[X]_{total}$ = 100 μM) were added to a buffered aqueous solution of bis-boronic receptor **1** at pH 7.4, and the emission intensity changes at 408 nm was recorded (Fig. 4A).

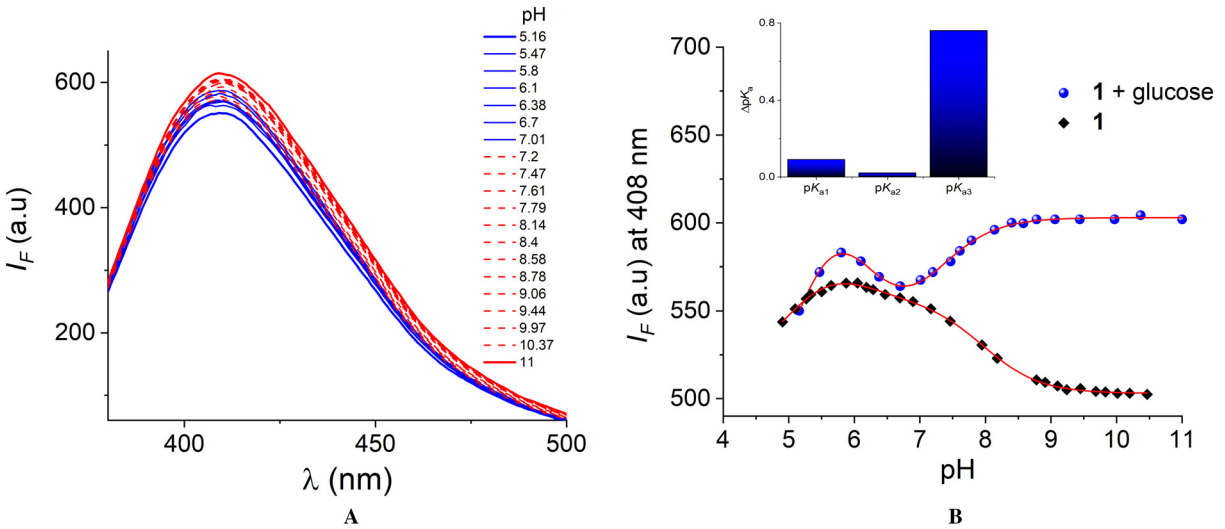

Fig. 3 (A) Fluorescence (λ_{ex} = 290 nm) pH titration of a buffered aqueous solution of **1** (5.0 μM) containing 10% vol of CH_3OH in the presence of 100 mM D-glucose. (B) Fluorimetric pH titration profiles at 408 nm of buffered aqueous solutions of **1** in the absence and presence of glucose (100 mM). The red solid lines represents the fits of the experimental data to the theoretical equation for three pK_a values.

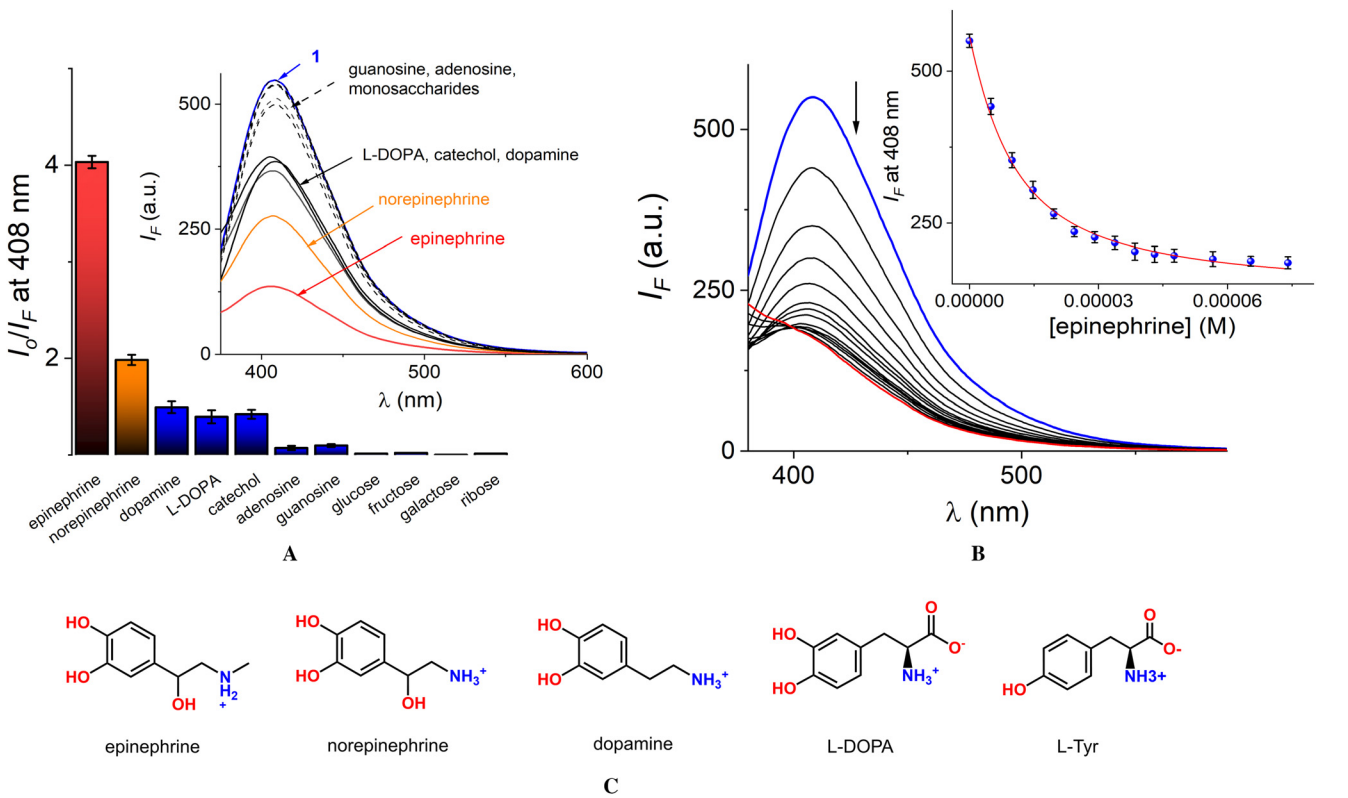

Fig. 4 (A) Fluorescence quenching at 408 nm (λ_{max} = 290 nm) of buffered (10 mM MOPS, pH = 7.4) aqueous solution of **1** (5 μM) containing 10 vol% of CH_3OH upon addition of NTs, nucleosides, monosaccharides, L-Tyr and catechol ($[analyte]_{total}$ = 100 μM). (B) Changes in the emission spectra of buffered aqueous solutions of **1** (containing 10% vol of CH_3OH) upon the addition of increasing amounts of epinephrine at pH 7.4. The inset shows the profile at 408 nm. The solid line represents the fit to eqn (1). (C) NTs used in this study.

Additions of nucleosides and monosaccharides induced only minor quenching, with I_F < 9% of their initial intensity I_0 at 408 nm. In contrast, the addition of dopamine, L-DOPA and catechol resulted in ~33% quenching of the fluorescence emission. Among the analytes tested, bis-boronic receptor **1** exhibited the strongest quenching response towards catecholamines bearing a hydroxyl group on the aliphatic side chain, such as epinephrine and norepinephrine, showing a pronounced turn-

off fluorescence of 78% and 46%, respectively. In Stern–Volmer coordinates, the selectivity towards epinephrine (I_o/I_F = 4.03) becomes more evident compared to the rest of the analytes (I_o/I_F < 1.98), including norepinephrine, dopamine and L-DOPA. Next, the binding affinities between **1** and epinephrine/norepinephrine were estimated *via* fluorimetric titration experiments (Fig. 4B and Fig. S18†). The titration profile for epinephrine fits well to a 1 : 1 binding model using the non-linear least-squares fitting of eqn (1), yielding an apparent biding constant of $K_{\mathbf{1}\text{-epi}} = (1.29 \pm 0.09) \times 10^5\ M^{-1}$.

$$\Delta I_{obs} = I_R + 0.5\Delta I_\infty \left\{ [A]_T + [R]_T + \frac{1}{K} - \left[\left([A]_T + [R]_T + \frac{1}{K} \right)^2 - [4][R]_T[A]_T \right]^{0.5} \right\} \quad (1)$$

where I_F is the observed intensity, I_R is the intensity of the free receptor, ΔI_∞ is the maximum change in intensity induced by the presence of the analyte at saturation, $[A]_T$ is the total analyte concentration, and K is the apparent binding constant. At saturation with epinephrine, the fluorescence intensity of **1** decreases by approximately fourfold. Fluorescence quenching of the aqueous solution of **1** induced by binding to epinephrine may originate from a photoinduced electron transfer (PET) mechanism, triggered by the formation of the sp^3-hybridized boronate anion.[3,39,79,80] The electron-rich catechol moiety typically acts as a PET-type quencher of boronic acid-appended organic fluorophores.[21]

Under the same conditions, apparent binding constants were determined for norepinephrine, dopamine, L-DOPA, L-Tyr and catechol for comparative purposes. The apparent complexation constant values are enlisted in Table 1, and the corresponding fitted fluorimetric titration curves at 408 nm are shown in Fig. 5A. All profiles fit well to a 1 : 1 binding model, with errors less than 10%. In contrast, fitting the data to a 1 : 2 model resulted in large errors, indicating that the two boronic acid units in **1** act as independent and simultaneous binding sites, each with similar binding constants and quenching responses.[62] In this case, the apparent binding constant K actually includes a statistical factor of 2.

This biding behavior is not unexpected because the separation between the two phenylboronic acid fragments is relatively large (>11 Å, *vide supra*), as observed in its crystal structure. In line with this, many bis-boronic glucose receptors with long spacers between boronic acid units act as simultaneous binding sites.[68,81–83]

An analysis of the performances of receptor **1** in terms of apparent binding constants towards NTs (Table 1) reveals the following selectivity trend: epinephrine > norepinephrine > dopamine, catechol, L-DOPA > L-Tyr. The two catecholamines containing an H-bond donor –OH group on their aliphatic chain (epinephrine and norepinephrine) exhibit the highest affinities, up to two orders of magnitude greater than those of analytes lacking this –OH group. Receptor **1** is approximately one order of magnitude more selective for epinephrine than for norepinephrine.

Table 1 Apparent binding constants $K_{1:1}$ (M^{-1}) for **1** and **2** with NTs and catechol in buffered aqueous solution

Receptor	Neurotransmitter	$K_{1:1}$	pH
1	Epinephrine	$(1.29 \pm 0.09) \times 10^5$	7.4
1	Epinephrine	$(1.55 \pm 0.05) \times 10^5$	8.0
1	Epinephrine	$(6.81 \pm 0.10) \times 10^4$	9.0
1	Norepinephrine	$(1.96 \pm 0.05) \times 10^4$	7.4
1	Dopamine	$(2.62 \pm 0.07) \times 10^4$	7.4
1	L-DOPA	$(2.03 \pm 0.03) \times 10^3$	7.4
1	Catechol	$(1.93 \pm 0.15) \times 10^3$	7.4
1	L-Tyr	$(5.98 \pm 0.20) \times 10^2$	7.4
2	Epinephrine	$(1.33 \pm 0.11) \times 10^3$	7.4

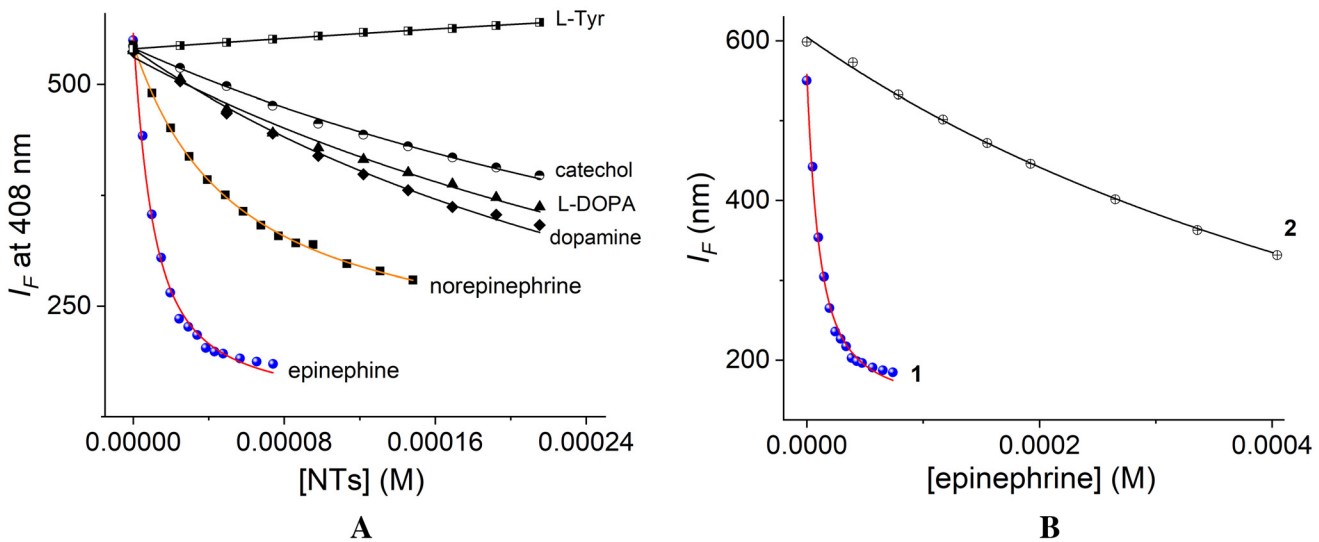

Fig. 5 Fluorimetric titrations (λ_{ex} = 290 nm) of aqueous solutions of (A) **1** (5 μM) at 408 nm and (B) **2** (10 μM) at 406 nm, each containing 10% vol of CH_3OH, upon the addition of increasing amounts of NTs and catechol at pH 7.4.

L-tyr, which lacks a catechol ring, shows the lowest binding affinity, suggesting that the catechol moiety is the primary recognition site. Therefore, in the design of boronic acid-based receptors for epinephrine, interference from amino acids is unlikely to pose a problem. This fact is remarkable because amino acids are often interfering species in receptor systems that rely on nucleophilic reactions involving the amino group.[44] Furthermore, to verify the esterification between the boronic acids and the catechol moiety of epinephrine, we measured the fluorescence response of reference compound **2**, which lacks boronic acid groups, under the same conditions as those used for bis-boronic receptor **1**. The observed quenching effect was markedly different, significantly smaller (Fig. 5B), and occurred without a shift in the emission maximum. The estimated apparent binding constant in this system, $K_{2\text{-epi}} = (1.33 \pm 0.11) \times 10^3$ M^{-1}, is two orders of magnitude lower than that observed for **1**, indicating weak association. This interaction likely arises only from hydrogen binding between the –OH/–NH groups of epinephrine and the imidazole rings of **2**.

Taking into account that complex formation between boronic acids and diols primarily occurs at pH ≥ pK_a of the tetrahedral boronate-based receptors, we also investigated the effect of pH on the quenching efficiency and binding affinity of **1** toward epinephrine at more basic pH values of 8 and 9.[64]

The fluorimetric titration profiles at 408 nm, along with the corresponding apparent binding constants obtained by fitting to a 1 : 1 model, are shown in Fig. S19† and Table 1.

In general, a modest pH-dependent quenching effect was observed across the range of pH 7.4 to 9.0. At pH 8.0, the estimated complexation constant between **1** and epinephrine is slightly higher than at the physiological pH of 7.4. This is not unexpected because the pK_a of **1** in the presence of a diol was estimated to be 7.21 (*vide supra*), and thus, pH values above this point yield affinity constants of a comparable order of magnitude. This result confirms that boronate groups are the primary interaction sites between **1** and epinephrine.

In contrast, at pH 9, the affinity of epinephrine for **1** is reduced by approximately one order of magnitude compared

Table 2 Apparent binding constants (log *K*) of dopamine and epinephrine complexes with mono- and bis-boronic receptors in aqueous media at pH 7.4

	Receptor	Dopamine	Epinephrine	Ref.
1	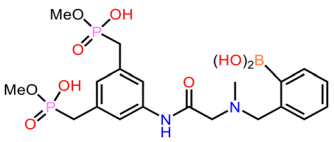	2.80	2.74	29
2	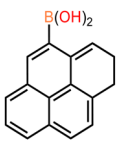	4.23	4.35	58
3	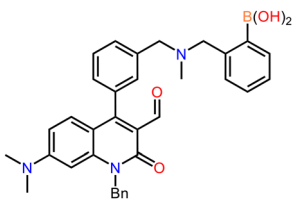	4.25	4.55	59
4	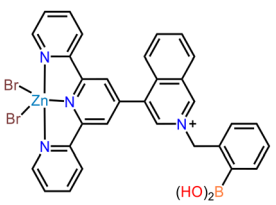	4.97	4.88	80
5	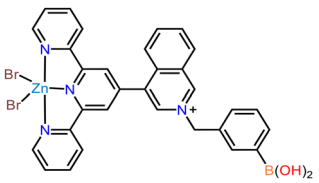	4.41	4.25	80
6	**1**	4.30	5.11	This work

to pH 7.4 and 8.0. This decrease can be attributed to the deprotonation of the ammonium group on the aliphatic chain of epinephrine, which hinders the formation of charge-assisted hydrogen bonds of the type $(Me)NH_2^+\cdots$N(imidazole) in the **1**-epinephrine complex.

To gain further insight into the nature of the quenching response induced by epinephrine, fluorescence lifetimes of aqueous solutions of **1** were measured in the absence and presence of epinephrine. A solution of **1** (5 μM), upon excitation with a 354 nm laser, exhibited a decay profile with a lifetime τ = 2.73 ns (Fig. S20†). The same solution with 5.0 equiv. of epinephrine showed a negligible change in lifetime value (τ = 2.59 ns), suggesting that the quenching is predominantly static and arises from complex formation with epinephrine (**1**-epinephrine).[62]

Table 2 summarizes the apparent binding constants of dopamine and epinephrine complexes for recently reported mono- and diboronic acid-based molecular receptors.[29,58,59] To date, all fluorescent molecular sensors/receptors have been of the mono-boronic type, with binding affinities in the range of log K = 2.80–4.41 and log K = 2.74–4.25 for dopamine and epinephrine, respectively. As observed from the values obtained using a single molecular recognition site based on the phenylboronic acid fragment, the selectivity between dopamine/epinephrine is practically non-existent (entries 1 and 2, Table 2).[29,58] In fact, when the receptor incorporates a second binding site specifically targeting the amino group, such as an aldehyde (entry 3, Table 2), the affinity is slightly higher for epinephrine, which contains a secondary amine. On the other hand, when the second association site is a metal center, as a Zn(II) atom, the affinity is modestly enhanced for dopamine, as observed in Zn(II)-terpyridine complexes (entries 4–5, Table 2). Among the molecular receptors reported for epinephrine to date,[29,58,59] receptor **1** has exhibits the highest affinity, which may result from cooperativity between multiple binding sites involving two boronic acid groups and two hydrogen bond acceptors, in contrast to mono-boronic acid-based receptors that possess only a single molecular recognition point.

Selective and fluorescent sensing performance for epinephrine

To probe the utility of bis-boronic chemosensor **1**, we determined the epinephrine concentration in a commercial pharmaceutical sample using fluorescence, as described below. Epinephrine was extracted from an aqueous pharmaceutical formulation (Piscaina, 50 mL, containing 0.005 mg mL^{-1} from PISA) by evaporation under reduced pressure to dryness and was subsequently re-dissolved in 1 mL of MilliQ ultra-pure water ($[epinephrine]_{final}$ = 1.36 mM). Aliquots of this solution (10 μL, 30 μL, 50 μL) were then added to 2.5 mL of a buffered aqueous solution of **1** (5 μM) containing 10 vol% of CH_3OH at pH = 7.4, and the emission intensity of the solution was recorded (Fig. S21†). The epinephrine concentration was calculated using the fitting equation derived from the fluorescence titration profile (inset, Fig. 4B). The fluorescent method using sensor **1** was validated by HPLC-UV quantification of epinephrine (Fig. S22†). A comparison of the epinephrine concentrations determined by fluorescent sensor **1** and HPLC-UV in water is shown in Fig. 6. The agreement between the two methods is excellent, with percentage recoveries ranging from 94% to 110%. It should be noted that the global commercial pharmaceutical formulations such as Piscaina contain competing species, some at millimolar concentrations (*e.g.*, lidocaine and D-glucose).

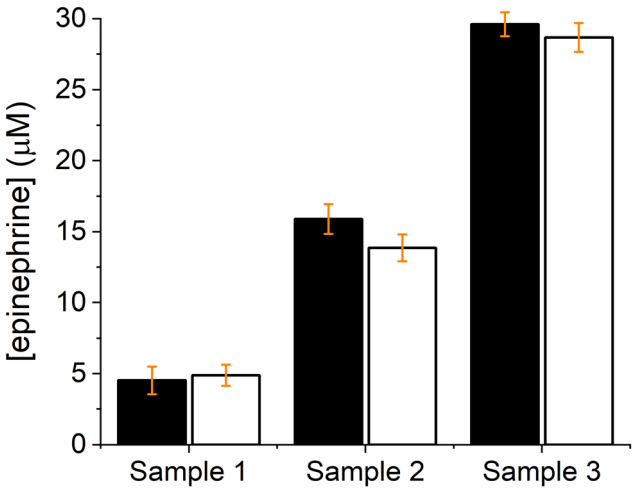

Fig. 6 Epinephrine concentrations determined from commercial pharmaceutical samples using fluorescent chemosensor **1** (black bars) and HPLC-UV (white bars). Measurements were carried out as described in the main text (average of triplicate experiments). The estimated error is ±1.0 μM.

For practical applications, luminescent epinephrine sensors must not only exhibit a good and rapid analytical response but also maintain selectivity in the presence of coexisting interfering molecules and ions found in physiological samples.[80] Therefore, a selectivity experiment was conducted for the diboronic receptor **1** against typical interfering species present in blood plasma and urine, such as creatinine, D-glucose, urea, L-proline, ATP, KCl, NaCl, NH_4Cl, $MgCl_2$ and NaF. The experiment was carried out at physiological pH under the same conditions as those used in Fig. 4B. Overall, the addition of these species ($[interference]_{total}$ = 1.0 mM, each one) to an aqueous solution of **1** (5 μM) induced a negligible change in its initial emission, as shown in Fig. 7A. In addition, Fig. 7B shows that the quenching response at 408 nm induced by epinephrine is not affected by the presence of typical background species from blood plasma and urine, thereby demonstrating the selectivity of the sensor even in the presence of potential biological interferences at millimolar concentrations.

Naked-eye ensemble for selective detection of epinephrine

Among the various chemosensing mechanisms for small molecules of biological or medicinal relevance, one of the most desirable systems is the so-called "naked-eye" sensing, in which the molecular recognition event produces a visible

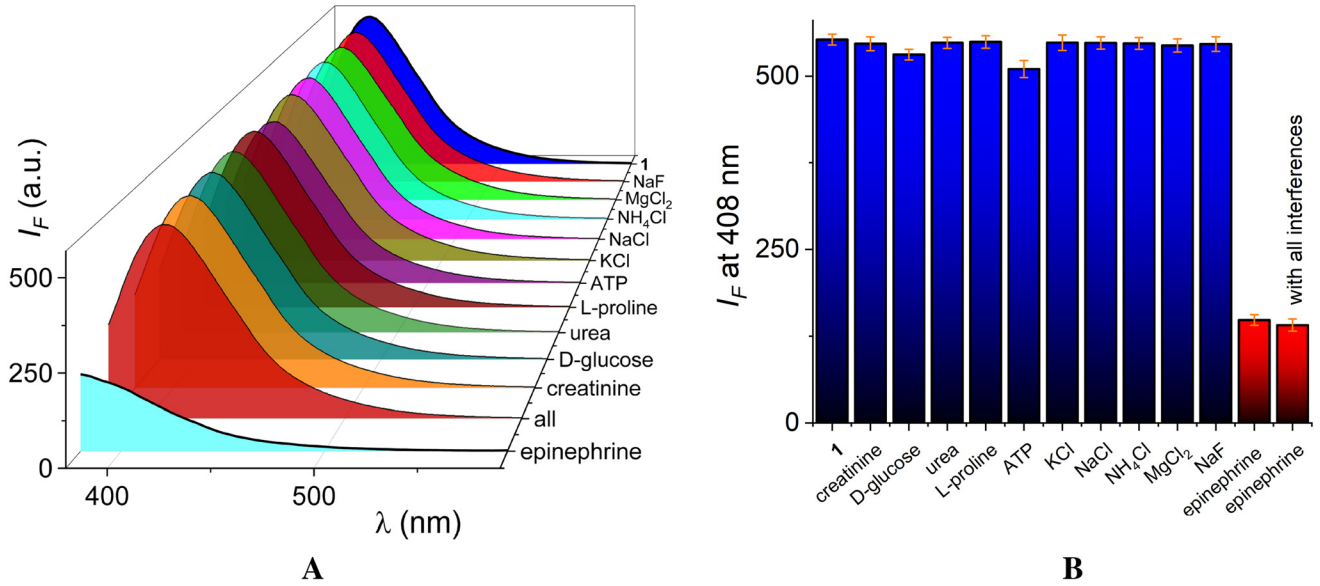

Fig. 7 Fluorescence spectra (λ_{ex} = 290 nm) (A) and emission intensities at 408 nm (B) of aqueous solutions of **1** (5 μM) containing 10 vol% of CH_3OH at pH 7.4 in the presence of various blood plasma and urine components ([interferent] = 1.0 mM, each).

color change without the need for additional analytical instruments.[84,85]

In this context, it is well known that Alizarin Red S (ARS) binds reversibly to phenyboronic acids ($K \sim 10^3$ M^{-1}) through its catechol ring and has been widely used to form chromogenic assemblies for the detection of sugars.[64,86] Therefore, we developed a visual sensing ensemble for the selective detection of epinephrine based on an *in situ* complex formed between the bis-boronic receptor **1** and the commercially available chromogenic indicator ARS.

Initially, we investigated the affinity of ARS (45 μM) for receptor **1** (0–95 μM) through a spectrophotometric titration experiment (Fig. 8A) in buffered water containing 10 vol% of CH_3OH at pH 7.4. Upon addition of **1**, the aqueous solution of ARS exhibited a rapid color change from red to orange, accompanied by a shift in the absorption maximum from 523 nm (free ASR, red) to 470 nm (esterification of the catechol ring of ARS with boronic acids, orange), as previously described by Wang.[64] Two isosbestic points at 491 nm and 640 nm were observed, indicating the presence of only two species in equilibrium (free ARS and the [ARS·**1**] complex). The titration profile at 523 nm was well fitted to a 1 : 1 binding model, yielding an apparent binding constant $K_{(ARS\text{-}1)}$ of (5.86 ± 0.05) × 10^4 M^{-1} (inset, Fig. 8A).

The affinity of **1** for ARS is one order of magnitude lower than that estimated for epinephrine but, importantly, is higher than that for NTs, monosaccharides and nucleosides tested, and is similar to that for norepinephrine. This makes the ARS·**1** ensemble a suitable candidate for selective chromogenic sensing of epinephrine.

On the other hand, upon the addition of epinephrine (up to 57 μM) to a buffered aqueous solution of the [ARS·**1**] ensemble (1 : 2 equiv.), the dye is rapidly displaced, and both the red color and the original absorbance spectrum of free ARS are nearly restored, as shown in Fig. 8B. The deep red color of the chromogenic ensemble enables real-time and selective detection of epinephrine by the naked eye in the micromolar concentration range. A comparison of the absorption spectra of the *in situ* [ARS·**1**] ensemble in the absence and presence of various analytes, such as epinephrine, dopamine, L-DOPA, norepinephrine, adenosine, fructose and catechol (Fig. 8C), reveals that only epinephrine can displace the dye. This selectivity can be attributed to the higher affinity of epinephrine for receptor **1**.

The selective and direct naked-eye detection of epinephrine using the chromogenic [ARS·**1**] ensemble is shown in Fig. 8D. To the best of our knowledge, this represents the first example of a naked-eye epinephrine sensing system capable of operating at the micromolar level.

Experimental-theoretical molecular recognition investigations

Molecular recognition mechanism of epinephrine by **1** was investigated using ^{11}B NMR spectroscopy, electrospray ionization mass spectrometry and DFT calculations. Evidence for the condensation between phenyl boronic acid moieties in **1** and the catechol group of epinephrine was directly obtained from ^{11}B NMR spectra recorded in a D_2O-CD_3OD mixture (v/v, 1 : 9). The ^{11}B NMR spectra of **1** (10 mM) in the absence and presence of 10 equiv. of epinephrine are shown in Fig. 9A. The single ^{11}B NMR signal observed for free **1** at δ = 28.01 ppm can be attributed to sp^2-hybridized B atoms. Upon addition of epinephrine, a strong upfield shift of the ^{11}B NMR signal to δ = 10.40 ppm is observed, which is characteristic of the conversion of trigonal planar, neutral sp^2 B atom to the tetrahedral, anionic sp^3 boronate form.[67]

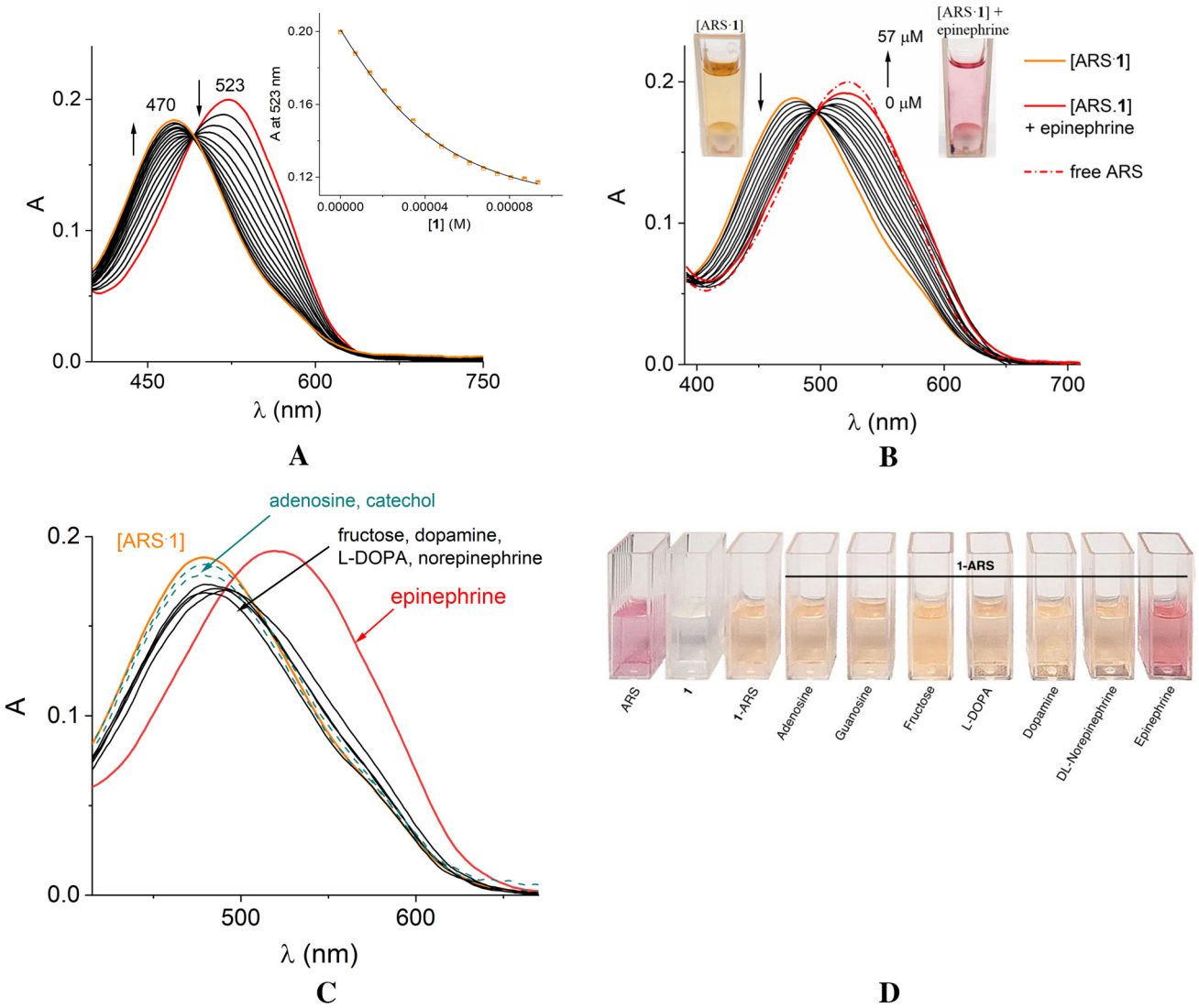

Fig. 8 (A) Changes in the absorbance of ARS (45 μM) upon the addition of **1** (0–95 μM). The inset shows the titration profile at 523 nm, and the solid line represents the fit to a 1 : 1 binding model. (B) Changes in the absorbance of the [ARS·**1**] complex (1 : 2) upon the addition of epinephrine (0–57 μM) in aqueous solution at pH 7.4 (10 mM MOPS) containing 10% vol of CH_3OH. (C) Absorption spectral changes of [ARS·**1**] in the presence of 60 μM of epinephrine and various analytes. (D) Naked-eye detection of epinephrine using a 1 : 2 mixture of ARS and 1 in aqueous CH_3OH at pH 7.4. Only epinephrine is capable to displace ARS from its complex with **1**, thereby restoring its color.

ESI-MS has previously been employed to study boronic acid–diol complexation.[62] In this study, electrospray ionization mass spectrometry was performed in the positive mode using a solution of **1** in the presence epinephrine (3 equiv.) at pH 7.4 in aqueous methanol (Fig. 9B). The resulting mass spectrum shows a signal at m/z = 909.2, separated by 1.0 m/z unit and isotopically resolved. This signal corresponds to the cationic 1 : 2 complex, {**1**·(epinephrine)$_2$ + H}$^+$, where receptor **1** forms two boronate esters through condensation with two epinephrine molecules, consistent with the ^{11}B NMR data. The characteristic isotopic pattern of this peak, arising from the presence of two B atoms (with two naturally occurring isotopes), confirms its identity.

To gain deeper insight into recognition mode of **1** towards epinephrine, DFT calculations were carried out for the 1 : 2 supramolecular complex. Initially, epinephrine is bound to receptor **1** *via* condensation of each catechol group with the boronate moieties, in agreement with the spectroscopic, ESI-MS, and ^{11}B NMR observations.

Thus, two possible supramolecular structures, **3** and **4** (Fig. S23†), were proposed for the {**1**·(epinephrine)$_2$} complex, differing in their H-bonding arrangements of type O–H···N$_{imidazole}$ and N–H···N$_{imidazole}$. Complex **3** features H-bonds between the hydroxyl groups of epinephrine and nitrogen atoms of the receptor, whereas complex **4** contains charged-assisted H-bonds involving the ammonium group of epinephrine and nitrogen atoms of the receptor.

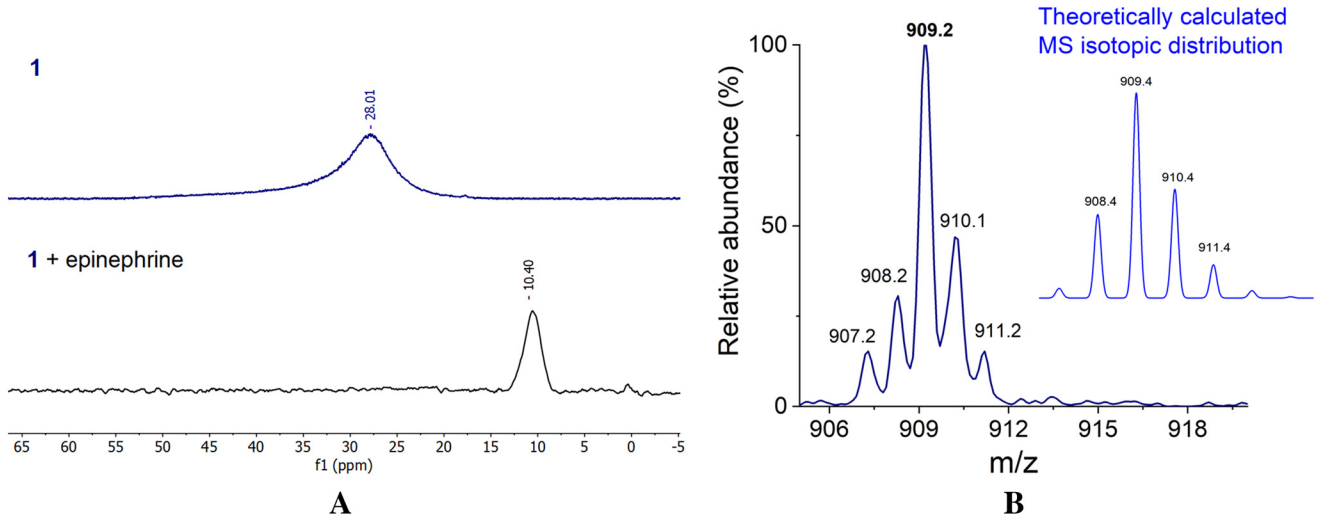

Fig. 9 (A) Change in the ^{11}B NMR spectrum (96 MHz, 25 °C) of **1** (10 mM) in the absence and presence of 10 equiv. of epinephrine in CD_3OD-D_2O (9 : 1, v/v). (B) Positive-mode ESI mass spectrum of an aqueous solution containing **1** and 3 equiv. of epinephrine. Inset: calculated isotopic distribution for the monocationic complex {**1**·(epinephrine)$_2$ + H^+}.

The geometry of the {**1**·(epinephrine)$_2$} complex was optimized at the B3LYP-D3BJ/def2-TZVP level of theory[87,88] with the implicit solvation model CPCM (water)[89] and the intermolecular interactions between **1** and epinephrine were characterized using the non-covalent interaction (NCI) index,[90] Atoms in Molecules (AIM) analysis[91] and interaction energies (see ESI† for computational methodology). The final structure is depicted in Fig. 10.

In this optimized model, each epinephrine molecule interacts with **1** through H-bonds of the type O–H···N or N–H···N. Notably, although the interaction between the two epinephrine molecules was not considered in the initial models, several intermolecular H-bonds were observed between them, providing a possible explanation for the selectivity of **1** towards epinephrine. Next, the geometry of the {**1**·(norepinephrine)$_2$} complex was also optimized for comparison purposes.

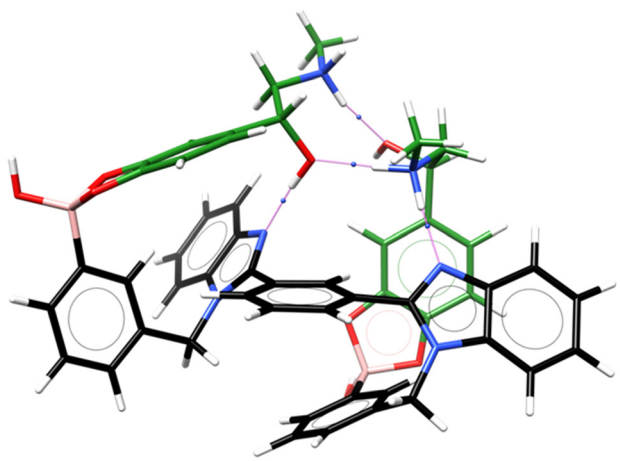

Fig. 10 Structure of the supramolecular model for the {**1**·(epinephrine)$_2$} complex optimized at the B3LYP-D3BJ/def2-TZVP level with the implicit solvation model CPCM (water). Epinephrine molecules are shown in green and receptor residue in black. The main interactions identified by AIM are indicated as pink paths, with blue dots representing BCPs.

The molecular structures of norepinephrine and epinephrine differ only by the substitution of an ammonium group with a methylammonium group; therefore, it is not surprising that the minimum-energy conformations of both complexes {**1**·(epinephrine)$_2$} and {**1**·(norepinephrine)$_2$} are quite similar (Fig. S24†).

This similarity also extends to the calculated interaction energies between **1** and epinephrine/norepinephrine, which are −53.61 kcal mol^{-1} and −51.31 kcal mol^{-1}, respectively. The slightly stronger interaction energy for the **1**-epinephrine complex supports the experimentally observed increase in binding constants.

To elucidate the nature of the interactions responsible for the increased affinity towards epinephrine, an AIM analysis was performed to identify and characterize all possible intermolecular interactions (Fig. 11A).

The parameters of the principal interactions found between **1**-NT complexes, where NT refers to epinephrine or norepinephrine, are summarized in Table 3. In both {**1**·(epinephrine)$_2$} and {**1**·(norepinephrine)$_2$} complexes, the main interactions exhibit a pattern in which receptor **1** acts as a hydrogen bond acceptor, while NT provides the hydrogen donor fragments –OH and –NH. The values of the electron density at the bond critical point, ρ(BCP), as well as the hydrogen bond distance (D_{AH}) and hydrogen bond interaction angle (θ_{AHD}), are nearly identical in both complexes. However, as shown by the NT–NT interactions (Table 4), an additional interaction of the H···H type, between the chiral hydrogen of one NT fragments and a hydrogen from the methylammonium group of the

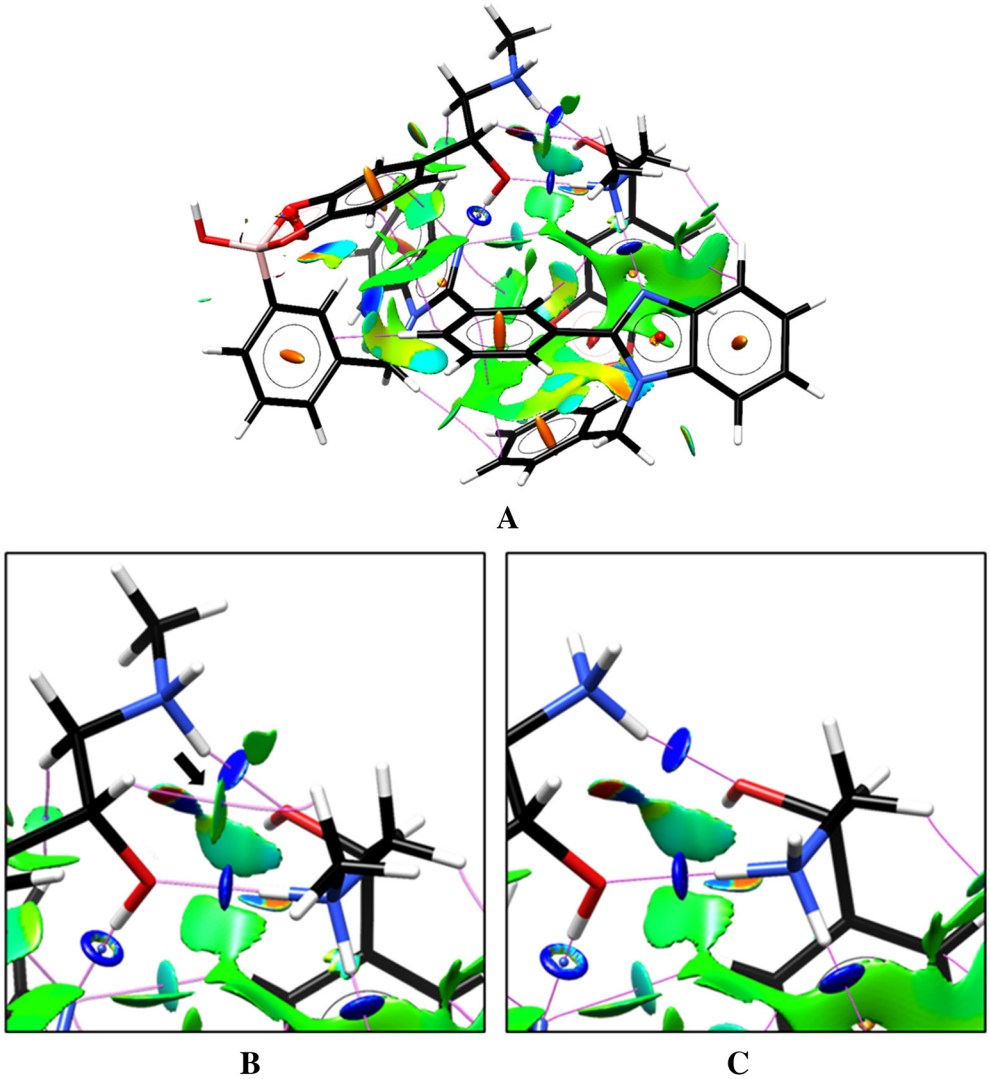

Fig. 11 (A) Non-covalent interaction (NCI) index and atoms in molecules (AIM) analysis for the optimized complex of **1** with epinephrine. Comparison between NCI and AIM analyses in the regions highlighted by dashed lines for the optimized complexes of **1** with epinephrine (B) and norepinephrine (C).

Table 3 Value of electron density at the bond critical point ρ(BCP), distance of hydrogen bond interactions (D_{AH}) and hydrogen bond interaction angles (θ_{AHD}) for interactions **1**-NT. N_R = imidazole ring of receptor **1**

Complex	IE	Interaction type	ρ(BCP)	D_{AH}	θ_{AHD}
{**1**·(epinephrine)$_2$}	−53.61	OH···N_R	0.05393	1.697	172.6
		NH···N_R	0.04269	1.813	162.5
{**1**·(norepinephrine)$_2$}	−51.31	OH···N_R	0.05339	1.702	173.1
		NH···N_R	0.04231	1.812	167.9

Table 4 Values of electron density at the bond critical point ρ(BCP), distance of hydrogen bond interactions (D_{AH}) and hydrogen bond interaction angles (θ_{AHD}) for NT–NT interactions

Complex	Interaction type	ρ(BCP)	D_{AH}	θ_{AHD}
{**1**·(epinephrine)$_2$}	O···HN	0.04329	1.725	166.2
	NH···O	0.03014	1.860	160.5
	H···H	0.02526	2.764	—
{**1**·(norepinephrine)$_2$}	O···HN	0.04411	1.713	171.7
	NH···O	0.03081	1.844	165.8

opposite NT fragment, can be observed in the **1**-epinephrine complex. Values of ρ(BCP), D_{AH} and θ_{AHD} indicate that this is a weaker interaction than a hydrogen bond. A non-covalent interaction analysis (Fig. 11B and C) reveals a small green isosurface associated with this H···H contact, which corresponds to a van der Waals interaction This interaction provides a plausible explanation for the increased interaction energy observed in the {**1**·(epinephrine)$_2$} complex.

Conclusions

We have developed a new fluorescent 1,3-bis-benzimidazole-benzene derivative bearing two phenyl boronic acid moieties, **1**, for the optical recognition of catecholamine-based neurotransmitters. This receptor **1**, exhibits high water solubility, photostability and the ability to sense epinephrine/norepinephrine at micromolar levels under physiological pH, through a rapid turn-off fluorescence response. Under these conditions, **1** showed particularly strong affinity for epinephrine ($K = 1.29 \times 10^5$ M^{-1}), with good selectivity over structurally related neurotransmitters such as dopamine, L-DOPA, and norepinephrine, as well as adenosine, guanosine, L-tyrosine and various monosaccharides. To date, bis-boronic acid compound **1** demonstrates the highest reported affinity for epinephrine binding by a molecular receptor.

Evidence from the X-ray crystal structure of **1**, pK_a values of boronic acids, fluorescence experiments, mass spectrometry, ^{11}B NMR measurements, DFT and AIM calculations indicate that epinephrine binds to **1** in a 1 : 2 mode *via* two-point recognition. This includes boronate–catechol condensation and multiple hydrogen bonds of the types OH···N and NH···N, formed between the aliphatic chain of epinephrine and imidazole ring of **1**, along with intermolecular interactions between the two epinephrine molecules in the final structure.

As a representative application, the epinephrine content in pharmaceutical samples was successfully quantified using fluorescence spectroscopy. Furthermore, the combination of bis-boronic acid **1** with the commercial Alizarin Red S dye can serve as an effective indicator displacement assay, enabling the visual detection of epinephrine by a distinct color change in the micromolar concentration range.

Overall, these results further highlight the potential of the new water-soluble and fluorescent bis-boronic acid receptor as an effective analytical tool for sensing epinephrine.

Experimental section

Reagents, solvents, and instrumentation are described in the ESI.†

Chemical synthesis

Intermediary L, 1,3-bis(1*H*-benzimidazole-2-yl)benzene, was synthesized following a previously reported procedure.[66]

Synthesis of (((1,3-phenylenebis(1*H*-benzo[*d*]imidazole-2,1-diyl))bis(methylene))bis(3,1-phenylene))diboronic acid, 1. A solution of L (50 mg, 0.16 mmol) in dry DMF (5 mL) was stirred with 2.1 equiv. of Cs_2CO_3 at r.t. for 1 h. Then, a solution of 3-(bromomethyl)phenylboronic acid (80.8 mg, 0.37 mmol) in dry DMF (1.0 mL) was added, and the reaction mixture was magnetically stirred for 18 h under an N_2 atmosphere. Subsequently, the reaction mixture was filtered through Celite, and the solvent was removed under reduced pressure. The addition of cold distillated H_2O afforded a white solid, which was collected by filtration, washed twice with distillated H_2O (10 mL) and recrystallized from THF : H_2O (9 : 1, v/v) to give **1** as colorless prismatic single crystals. Yield: 83.1% (77.5 mg).

^{1}H NMR (300 MHz, MeOD) δ: 7.96 (t, J = 1.7 Hz, 1H), 7.88 (dd, J = 7.5, 1.9 Hz, 2H), 7.77–7.66 (m, 3H), 7.56–7.48 (m, 2H), 7.46–7.41 (m, 2H), 7.37–7.27 (m, 6H), 7.20 (t, J = 7.6 Hz, 2H), 7.00–6.91 (m, 2H), 5.50 (s, 4H).

^{13}C NMR (75 MHz, 25 °C, CD_3OD) δ: 179.14, 152.88, 141.99, 135.71, 135.40, 132.84, 131.35, 130.84, 130.41, 129.80, 129.38, 127.83, 127.45, 123.37, 122.85, 118.64, 110.91. The signal corresponding to methylene (–CH_2–) group overlaps with the solvent signal. **^{11}B NMR** (96 MHz, 298 K, CD_3OD): δ = 28.91 ppm. **ESI(–)-MS** (m/z): calculated for $C_{44}H_{50}B_2N_4O_7$, {**1**-$(OMe)_2$ + 2(THF) + (H_2O) + H}$^+$: 768.53; found: 768.9. **ATR-IR** (cm^{-1}): 3050 (f), 2978 (f), 2872 (f), 1348 (m, B–O), 1329 (m, C–B), 739 (s), 709 (s). Elem. anal. calcd for the X-ray crystalline sample {**1** + 3(THF)}, {$C_{34}H_{28}B_2N_4O_4$ + 3(C_4H_8O)}; C, 69.54; H, 6.60; N, 7.05; found: C, 69.39; H, 6.77; N, 6.91.

Synthesis of 1,3-bis(1-benzyl-1*H*-benzo[*d*]imidazol-2-yl) benzene, 2. It was obtained following the same procedure as for **1**, using 3.0 equiv. of benzyl bromide instead of 3-(bromomethyl)phenylboronic acid. Colorless single crystals suitable for X-ray diffraction were obtained by slow solvent evaporation from a methanolic solution at r.t. Yield: 87.5% (70 mg).

^{1}H NMR (500 MHz, 25 °C, DMSO-d_6) δ: 8.14 (t, J = 1.8 Hz, 1H), 7.87 (dd, J = 7.8, 1.7 Hz, 2H), 7.77–7.72 (m, 2H), 7.68 (t, J = 7.8 Hz, 1H), 7.53–7.46 (m, 2H), 7.28–7.18 (m, 10H), 6.97–6.92 (m, 4H), 5.57 (s, 4H).

^{13}C NMR (125 MHz, 25 °C, DMSO-d_6) δ (in ppm): 152.55, 142.64, 136.81, 135.97, 130.78, 130.35, 129.90, 129.53, 128.85, 127.64, 126.26, 123.07, 122.52, 119.46, 111.33, 47.58. DART (+)-MS (m/z): calculated for $C_{34}H_{27}N_4$, {**2** + H}$^+$, 491.62; found: 491. IR-ATR (cm^{-1}): ν = 3029 (f, sp^2-CH), 2910 (f, sp^3-CH), 2872 (f), 1449 (m, C=C), 749 (s), 706 (s). Elem. anal. calcd for the X-ray crystalline sample $C_{34}H_{26}N_4$ (490.61): C, 83.24; H, 5.34; N, 11.42; found: C, 82.98; H, 5.41; N, 11.33.

X-ray crystallographic investigations

Data for **1** and **2** were collected on a Bruker APEX II CCD diffractometer at 100 K, using Mo-Kα radiation (λ = 0.71073 Å) for **1** and Cu-Kα radiation (λ = 1.54178 Å) for **2**, both from Incoatec ImuS sources with a Helios optic monochromator. Suitable crystals were coated with hydrocarbon oil, mounted on a nylon loop, and placed in a cold nitrogen stream on the diffractometer. Frames were collected using ω scans and integrated with SAINT.[92] A multi-scan absorption correction (SADABS) was applied.[92] The structures were solved by direct methods and refined by full-matrix least-squares on F^2 using SHELXL-2018[93] *via* the SHELXLE GUI.[94] In compound **1**, the THF molecule was modeled using SIMU, RIGU and SAME instructions implemented in SHELXLE GUI,[94] and the occupancy was refined using a free variable The hydrogen atoms bonded to carbon (C–H) were placed in idealized positions, while hydrogen atoms of the O–H moiety were located in the residual electron density map and refined with U_{iso} = $_aU_{eq}$ (where a is 1.5 for –CH_3 and –OH moieties, and 1.2 for all others).

Compound **1** crystallized in the triclinic system, in the *P* space group. It crystallized as a solvate, where one THF molecule exhibits positional disorder, modeled in two positions. The major occupancy site was refined to 85%.

Compound **2** crystallized in the orthorhombic system, in the chiral $P2_12_12_1$ space group. Considering the chiral space group and the atomic composition, where nitrogen is the heaviest atom, data were collected using copper radiation. The absolute structure parameter was determined using the Parsons-Flack method, yielding a value of 0.00(12). Crystallographic data for both crystal structures have been deposited with the Cambridge Crystallographic Data Centre under CCDC numbers 2252384–2252385.† X-ray crystallographic files in CIF format for complexes **1** and **2** are available free of charge in the ESI.†

Conflicts of interest

There are no conflicts to declare.

Data availability

Crystallographic data for compounds **1** and **2** have been deposited at the Cambridge Crystallographic Data Centre under CCDC numbers 2252384–2252385.†

Acknowledgements

We thank M. Sc. Eréndira García Rios, M. Sc. Lucero Mayra Ríos Ruiz, M. Sc. Lucía del Carmen Márquez Alonso, M. Sc. Lizbeth Triana Cruz, Dr Beatriz Quiroz-García, Dr. Adriana Romo Pérez, M. Sc. Elizabeth Huerta Salazar, Chem. María de la Paz Orta Pérez, M.Sc, Mayra León Santiago and Dr. Francisco Javier Pérez Flores for technical assistance. We thank PAPIIT-UNAM 200023 for financial support. A. O. V.-P. is grateful to SECIHTI for doctoral scholarship 868013.

References

1 P. Jana and S. Bandyopadhyay, Optical Sensor Arrays for the Detection of Neurotransmitters, *Analysis Sensing*, 2024, **4**, e202300099.
2 T. Pradhan, H. S. Jung, J. H. Jang, T. W. Kim, C. Kang and J. S. Kim, Chemical sensing of neurotransmitters, *Chem. Soc. Rev.*, 2014, **43**, 4684–4713.
3 R. Govindaraju, S. Govindaraju, K. Yun and J. Kim, Fluorescent-Based Neurotransmitter Sensors: Present and Future Perspectives, *Biosensors*, 2023, **13**, 1008.
4 J. Krämer, R. Kang, L. M. Grimm, L. De Cola, P. Picchetti and F. Biedermann, Molecular Probes, Chemosensors, and Nanosensors for Optical Detection of Biorelevant Molecules and Ions in Aqueous Media and Biofluids, *Chem. Rev.*, 2022, **122**, 3459–3636.
5 Y. Ou, A. M. Buchanan, C. E. Witt and P. Hashemi, Frontiers in electrochemical sensors for neurotransmitter detection: Towards measuring neurotransmitters as chemical diagnostics for brain disorders, *Anal. Methods*, 2019, **11**, 2738–2755.
6 F. Ghasemi, M. R. Hormozi-Nezhad and M. Mahmoudi, Identification of catecholamine neurotransmitters using fluorescence sensor array, *Anal. Chim. Acta*, 2016, **917**, 85–92.
7 N. C. Spitzer, Neurotransmitter Switching in the Developing and Adult Brain, *Annu. Rev. Neurosci.*, 2017, **40**, 1–19.
8 G. Ayano, Common Neurotransmitters : Criteria for Neurotransmitters, Key Locations, Classifications and Functions, *Am. J. Psychiatry Neurosci.*, 2017, **4**, 91–95.
9 G. Eisenhofer, I. J. Kopin and D. S. Goldstein, Catecholamine metabolism: A contemporary view with implications for physiology and medicine, *Pharmacol. Rev.*, 2004, **56**, 331–349.
10 M. Tsunoda, Recent advances in methods for the analysis of catecholamines and their metabolites, *Anal. Bioanal. Chem.*, 2006, **386**, 506–514.
11 L. Duan and Y. Zhao, Selective Binding of Dopamine and Epinephrine in Water by Molecularly Imprinted Fluorescent Receptors, *Chem. – Asian J.*, 2020, **15**, 1035–1038.
12 C. H. Mak, C. Liao, Y. Fu, M. Zhang, C. Y. Tang, Y. H. Tsang, H. L. W. Chan and F. Yan, Highly-sensitive epinephrine sensors based on organic electrochemical transistors with carbon nanomaterial modified gate electrodes, *J. Mater. Chem. C*, 2015, **3**, 6532–6538.
13 K. E. Barrett, S. M. Barman, S. Boitano and H. L. Brooks, *Review of medical physiology*, Mc Graw Hill/Lange, 2010, p. 23.
14 S. D. Niyonambaza, P. Kumar, P. Xing, J. Mathault, P. De Koninck, E. Boisselier, M. Boukadoum and A. Miled, A review of neurotransmitters sensing methods for neuroengineering research, *Appl. Sci.*, 2019, **9**, 1–31.
15 Y. Zhao, Y. Mei, J. Sun and Y. Tian, A Supramolecular Fluorescent Chemosensor Enabling Specific and Rapid Quantification of Norepinephrine Dynamics, *J. Am. Chem. Soc.*, 2025, **147**, 5025–5034.
16 A. Bhattacharya, K. B. Patel, R. Ghosh, D. N. Srivastava and P. B. Chatterjee, Chemical Interference-free multimodal biosensing of adrenaline over other neurotransmitters : Role of 2-iminomethylenephenylboronic acid as the signal transduction unit of fluorescence and impedance, *Sens. Actuators, B*, 2024, **398**, 134772.
17 K. J. Broadley, The vascular effects of trace amines and amphetamines, *Pharmacol. Ther.*, 2010, **125**, 363–375.
18 N. Chauhan, S. Soni, P. Agrawal, Y. P. S. Balhara and U. Jain, Recent advancement in nanosensors for neurotransmitters detection: Present and future perspective, *Process Biochem.*, 2019, **91**, 241–259.
19 J. Kim, B. Raman and K. H. Ahn, Artificial receptors that provides a preorganized hydrophobic environment: A bio-

mimetic approach to dopamine recognition in water, *J. Org. Chem.*, 2006, **71**, 38–45.
20 D. Merims and N. Giladi, Dopamine dysregulation syndrome, addiction and behavioral changes in Parkinson's disease, *Parkinsonism Relat. Disord.*, 2008, **14**, 273–280.
21 K. E. Secor and T. E. Glass, Selective amine recognition: development of a chemosensor for dopamine and norepinephrine, *Org. Lett.*, 2004, **6**, 3727–3730.
22 D. L. Wong, T. C. Tai, D. C. Wong-Faull, R. Claycomb, E. G. Meloni, K. M. Myers, W. A. Carlezon and R. Kvetnansky, Epinephrine: A short- and long-term regulator of stress and development of illness: A potential new role for epinephrine in stress, *Cell. Mol. Neurobiol.*, 2012, **32**, 737–748.
23 S. Yadav, M. A. Sadique, S. Singhai and R. Khan, Rapid electrochemical detection of epinephrine in human serum based on polydopamine-wrapped cerium oxide nanocomposite, *Hybrid Adv.*, 2023, **4**, 100108.
24 N. G. Mphuthi, A. S. Adekunle and E. E. Ebenso, Electrocatalytic oxidation of Epinephrine and Norepinephrine at metal oxide doped phthalocyanine/MWCNT composite sensor, *Sci. Rep.*, 2016, **6**, 1–20.
25 C. Wang, Q. Han, P. Liu, G. Zhang, L. Song, X. Zou and Y. Fu, A Superstable Luminescent Lanthanide Metal Organic Gel Utilized in an Electrochemiluminescence Sensor for Epinephrine Detection with a Narrow Potential Sweep Range, *ACS Sens.*, 2021, **6**, 252–258.
26 S. Koppayithodi, P. Jana and S. Bandyopadhyay, Highly Selective and Quantitative Point-of-Care Diagnostic Method for Adrenaline, *Chem. – Eur. J.*, 2023, **29**, e202300327.
27 S. Pal, M. Jana, M. Chowdhury and P. Kumar Das, Selective Sensing of Epinephrine by Phenylboronic Acid Tethered Carbon Dot, *Chem. – Asian J.*, 2023, **18**, e202300415.
28 M. Zhang, Y. Wang, J. Jiang, Y. Jiang and D. Song, The Role of Catecholamines in the Pathogenesis of Diseases and the Modified Electrodes for Electrochemical Detection of Catecholamines: A Review, *Crit. Rev. Anal. Chem.*, 2024, 1–22.
29 M. Maue and T. Schrader, A color sensor for catecholamines, *Angew. Chem., Int. Ed.*, 2005, **44**, 2265–2270.
30 J. W. Pearson and J. S. Redding, The Role of Epinephrine in Cardiac Resuscitation., *Anesth. Analg.*, 1963, **42**, 599–606.
31 K. Stroumpoulis, T. Xanthos, G. Rokas, V. Kitsou, D. Papadimitriou, I. Serpetinis, D. Perrea, L. Papadimitriou and E. Kouskouni, Vasopressin and epinephrine in the treatment of cardiac arrest: An experimental study, *Crit. Care*, 2008, **12**, 1–6.
32 H. Ge, Q. Ye, T. Zou, D. Zhang, H. Liu and R. Yang, Recent progress of molecular fluorescent probes with multi-recognition sites enable sensitive and selective analysis, *TrAC, Trends Anal. Chem.*, 2024, **174**, 117685.
33 A. Palta, D. Singla, K. Paul and V. Luxami, Coumarin––Pyrazole Based Fluorescent Sensor for Selective Detection of Dopamine in Aqueous Medium, *ChemistrySelect*, 2023, **8**, e202301864.
34 X. Liu and J. Liu, Biosensors and sensors for dopamine detection, *View*, 2021, **2**, 1–16.
35 A. Kumar, A. Kumari, P. Mukherjee, T. Saikia, K. Pal and S. K. Sahu, A design of fluorescence-based sensor for the detection of dopamine via FRET as well as live cell imaging, *Microchem. J.*, 2020, **159**, 105590.
36 X. Z. Dong, Z. Sun, L. Han, Y. Ling, B. L. Li, N. B. Li and H. Q. Luo, A "traffic light" signal ratiometric fluorescence sensor for highly sensitive and selective detection of dopamine, *Sens. Actuators, B*, 2022, **372**, 132668.
37 F. B. Kammal-Eddin and Y. Wing-Fen, Recent Advances in Electrochemical and Optical Sensing of Dopamine, *Sensors*, 2020, **20**, 1–47.
38 F. Moghzi, J. Soleimannejad, E. C. Sañudo and J. Janczak, Dopamine Sensing Based on Ultrathin Fluorescent Metal-Organic Nanosheets, *ACS Appl. Mater. Interfaces*, 2020, **12**, 44499–44507.
39 K. S. Hettie and T. E. Glass, Coumarin-3-aldehyde as a scaffold for the design of tunable PET-modulated fluorescent sensors for neurotransmitters, *Chem. – Eur. J.*, 2014, **20**, 17488–17499.
40 B. Si and E. Song, Recent advances in the detection of neurotransmitters, *Chemosensors*, 2018, **6**, 1–24.
41 Y. Ding, K. Tan, S. Zhang, S. Wang, X. Zhang and P. A. Hu, Wearable and recyclable epinephrine biosensors based on molecular imprinting polymer modified organic electrochemical transistors, *Chem. Eng. J.*, 2023, **477**, 146844.
42 N. Lavanya, E. Fazio, F. Neri, A. Bonavita, S. G. Leonardi, G. Neri and C. Sekar, Simultaneous electrochemical determination of epinephrine and uric acid in the presence of ascorbic acid using SnO2/graphene nanocomposite modified glassy carbon electrode, *Sens. Actuators, B*, 2015, **221**, 1412–1422.
43 S. Ali, S. Sikdar, S. Basak, M. S. Haydar, K. Mallick, M. Mondal, D. Roy, S. Ghosh, S. Sahu, P. Paul and M. N. Roy, Label-Free Detection of Epinephrine Using Flower-like Biomimetic CuS Antioxidant Nanozymes, *Inorg. Chem.*, 2023, **62**, 11291–11303.
44 S. Baluta, K. Malecha, A. Świst and J. Cabaj, Fluorescence sensing platforms for epinephrine detection based on low temperature cofired ceramics, *Sensors*, 2020, **20**, 1429.
45 Y. Zhang, W. Ren, Y. Z. Fan, H. Q. Luo and N. B. Li, Chemically-modulated turn-on fluorescence for rapid and visual discrimination of norepinephrine and epinephrine and its application for dopamine-β-hydroxylase detection, *Sens. Actuators, B*, 2020, **305**, 127463.
46 Z. Liu and S. Liu, A novel fluorescent biosensor for adrenaline detection and tyrosinase inhibitor screening, *Anal. Bioanal. Chem.*, 2018, **410**, 4145–4152.
47 S. Huang, M. He, S. Jiang, G. Su, Z. Lu, T. Liu, C. Wu, X. Wang, Y. Wang, X. Zhao, C. Song, H. Rao and M. Sun, Electron-regulated WO3/Mn3O4 bi-enzyme activity for colorimetric detection epinephrine with smartphones, *Sens. Actuators, B*, 2023, **390**, 134009.
48 D. Das and R. K. Dutta, Ethylene glycol and alanine anhydride based nitrogen doped fluorescent carbon nanoparticles as probe for detection of epinephrine, nor-epinephrine and dopamine, *Dyes Pigm.*, 2022, **203**, 110314.

49 W. Wu, L. Ding, H. Lin, Z. Xia, S. Yu and J. Huang, A highly sensitive fluorescence sensor for adrenaline detection based on modified carbon quantum dots, *Proc. SPIE*, 2018, **10964**, 258.
50 W. Liu, F. Cui, H. Li, S. Wang and B. Zhuo, Three-dimensional hybrid networks of molecularly imprinted poly(9-carbazoleacetic acid) and MWCNTs for simultaneous voltammetric determination of dopamine and epinephrine in plasma sample, *Sens. Actuators, B*, 2020, **323**, 128669.
51 G. Mi, M. Yang, C. Wang, B. Zhang, X. Hu, H. Hao and J. Fan, A simple "turn off-on" ratio fluorescent probe for sensitive detection of dopamine and lysine/arginine, *Spectrochim. Acta, Part A*, 2021, **253**, 119555.
52 F. Wei, G. Xu, Y. Wu, X. Wang, J. Yang, L. Liu, P. Zhou and Q. Hu, Molecularly imprinted polymers on dual-color quantum dots for simultaneous detection of norepinephrine and epinephrine, *Sens. Actuators, B*, 2016, **229**, 38–46.
53 S. Govindaraju, A. S. Reddy, J. Kim and K. Yun, Sensitive detection of epinephrine in human serum via fluorescence enhancement of gold nanoclusters, *Appl. Surf. Sci.*, 2019, **498**, 143837.
54 N. Saraf, A. Bosak, A. Willenberg, S. Das, B. J. Willenberg and S. Seal, Colorimetric detection of epinephrine using an optimized paper-based aptasensor, *RSC Adv.*, 2017, **7**, 49133–49143.
55 M. A. Mohsin, B. D. Liu, X. L. Zhang, W. J. Yang, L. S. Liu and X. Jiang, Cellular-membrane inspired surface modification of well aligned ZnO nanorods for chemosensing of epinephrine, *RSC Adv.*, 2017, **7**, 3012–3020.
56 A. Prasanna de Silva, H. Q. Nimal-Gunaratne, T. Gunnlaugsson, A. J. M. Huxley, C. P. McCoy, J. T. Rademacher and T. E. Rice, Signaling Recognition Events with Fluorescent Sensors and Switches, *Chem. Rev.*, 1997, **97**, 1515–1566.
57 C. Luo, Y. Chen, J. Gu, H. Cai, H. Lin, Z. Jin and C. Huang, Activatable NIR Fluorescence Probe for Epinephrine Detection and Bioimaging Based on Anionic Heptamethine Cyanine, *Anal. Chem.*, 2024, **96**, 9969.
58 A. Chaicham, S. Sahasithiwat, T. Tuntulani and B. Tomapatanaget, Highly effective discrimination of catecholamine derivatives via FRET-on/off processes induced by the intermolecular assembly with two fluorescence sensors, *Chem. Commun.*, 2013, **49**, 9287–9289.
59 L. Zhang, X. A. Liu, K. D. Gillis and T. E. Glass, A High-Affinity Fluorescent Sensor for Catecholamine: Application to Monitoring Norepinephrine Exocytosis, *Angew. Chem., Int. Ed.*, 2019, **58**, 7611–7614.
60 G. F. Whyte, R. Vilar and R. Woscholski, Molecular recognition with boronic acids-applications in chemical biology, *J. Chem. Biol.*, 2013, **6**, 161–174.
61 X. Wu, X. X. Chen and Y. B. Jiang, Recent advances in boronic acid-based optical chemosensors, *Analyst*, 2017, **142**, 1403–1414.
62 J. Valdes-García, J. Zamora-Moreno, M. K. Salomón-Flores, D. Martínez-Otero, J. Barroso-Flores, A. K. Yatsimirsky, I. J. Bazany-Rodríguez and A. Dorazco-González, Fluorescence Sensing of Monosaccharides by Bis-boronic Acids Derived from Quinolinium Dicarboxamides: Structural and Spectroscopic Studies, *J. Org. Chem.*, 2023, **88**, 2174–2189.
63 L. R. Ortega-Valdovinos, J. Valdes-García, I. J. Bazany-Rodríguez, J. C. Lugo-González, A. Dorazco-González and A. K. Yatsimirsky, Anion recognition by anthracene appended ortho -aminomethylphenylboronic acid: a new PET-based sensing mechanism, *New J. Chem.*, 2021, **45**, 15618–15628.
64 G. Springsteen and B. Wang, A detailed examination of boronic acid-diol complexation, *Tetrahedron*, 2002, **58**, 5291–5300.
65 M. Herm, O. Molt and T. Schrader, Towards synthetic adrenaline receptors-shape-selective adrenaline recognition in water, *Angew. Chem., Int. Ed.*, 2001, **40**, 3148–3151.
66 J. Valdes-García, A. O. Viviano-Posadas, J. Rivera-Chávez, T. Ramírez-Apan, S. Martínez-Vargas, E. Aguirre-Hernández, J. M. German-Acacio, D. Morales-Morales and A. Dorazco-González, Crystal structures and study of interaction mode of bis-benzimidazole-benzene derivatives with DNA, *J. Mol. Struct.*, 2022, **1249**, 131582.
67 S. A. Valenzuela, J. R. Howard, H. M. Park, S. Darbha and E. V. Anslyn, 11B NMR Spectroscopy: Structural Analysis of the Acidity and Reactivity of Phenyl Boronic Acid-Diol Condensations, *J. Org. Chem.*, 2022, **87**, 15071–15076.
68 S. Gamsey, N. A. Baxter, Z. Sharrett, D. B. Cordes, M. M. Olmstead, R. A. Wessling and B. Singaram, The effect of boronic acid-positioning in an optical glucose-sensing ensemble, *Tetrahedron*, 2006, **62**, 6321–6331.
69 X. Wu, Z. Li, X.-X. Chen, J. S. Fossey, T. D. James and Y.-B. Jiang, Selective sensing of saccharides using simple boronic acids and their aggregates, *Chem. Soc. Rev.*, 2013, **42**, 8032–8048.
70 M. M. Quesada-Moreno, A. J. Cruz-Cabeza, J. R. Avilés-Moreno, P. Cabildo, R. M. Claramunt, I. Alkorta, J. Elguero, F. J. Zúñiga and J. J. López-González, The Curious Case of 2-Propyl-1H-benzimidazole in the Solid State: An Experimental and Theoretical Study, *J. Phys. Chem. A*, 2017, **121**, 5665–5674.
71 P. R. Spackman, M. J. Turner, J. J. McKinnon, S. K. Wolff, D. J. Grimwood, D. Jayatilaka and M. A. Spackman, CrystalExplorer: A program for Hirshfeld surface analysis, visualization and quantitative analysis of molecular crystals, *J. Appl. Crystallogr.*, 2021, **54**, 1006–1011.
72 M. A. Spackman and J. J. McKinnon, Fingerprinting intermolecular interactions in molecular crystals, *CrystEngComm*, 2002, **4**, 378–392.
73 I. D. Madura, K. Czerwińska and D. Sołdańska, Hydrogen-bonded dimeric synthon of fluoro-substituted phenylboronic acids versus supramolecular organization in crystals, *Cryst. Growth Des.*, 2014, **14**, 5912–5921.
74 N. Shtemenko, C. Galiana-Rosello, A. Gil-Martínez, S. Blasco, J. Gonzalez-García, H. Velichko, O. Holichenko, O. Shtemenko and E. García-España, Two rhenium com-

pounds with benzimidazole ligands: synthesis and DNA interactions, *RSC Adv.*, 2024, **14**, 19787–19793.
75 W. L. A. Brooks, C. C. Deng and B. S. Sumerlin, Structure-Reactivity Relationships in Boronic Acid-Diol Complexation, *ACS Omega*, 2018, **3**, 17863–17870.
76 G. Jerez, G. Kaufman, M. Prystai, S. Schenkeveld and K. K. Donkor, Determination of thermodynamic pKa values of benzimidazole and benzimidazole derivatives by capillary electrophoresis, *J. Sep. Sci.*, 2009, **32**, 1087–1095.
77 L. Antonov, S. Kawauchi and K. Shirata, Acid Dissociation Constants of the Benzimidazole Unit in the Polybenzimidazole Chain: Configuration Effects, *Molecules*, 2022, **27**, 1–22.
78 B. Wang, K. H. Chou, B. N. Queenan, S. Pennathur and G. C. Bazan, Molecular Design of a New Diboronic Acid for the Electrohydrodynamic Monitoring of Glucose, *Angew. Chem., Int. Ed.*, 2019, **58**, 10612–10615.
79 M. K. Salomón-Flores, A. O. Viviano-Posadas, J. Valdes-García, V. López-Guerrero, D. Martínez-Otero, J. Barroso-Flores, J. M. German-Acacio, I. J. Bazany-Rodríguez and A. Dorazco-González, Optical sensing of l-dihydroxy-phenylalanine in water by a high-affinity molecular receptor involving cooperative binding of a metal coordination bond and boronate-diol, *Dalton Trans.*, 2024, **53**, 16541–16556.
80 I. J. Bazany-Rodríguez, M. K. Salomón-Flores, A. O. Viviano-Posadas, M. A. García-Eleno, D. Martínez-Otero and A. Dorazco-González, Chemosensing of neurotransmitters with selectivity and naked eye detection of L-DOPA based on fluorescent Zn(II)-terpyridine bearing boronic acid complexes, *Dalton Trans.*, 2021, **50**, 4255–4269.
81 J. Zamora-Moreno, M. K. Salomón-Flores, J. Valdes-García, C. Pinzón-Vanegas, D. Martínez-Otero, J. Barroso-Flores, R. Villamil-Ramos, M. A. Romero-Solano and A. Dorazco-González, Water-soluble fluorescent chemosensor for sorbitol based on a dicationic diboronic receptor. Crystal structure and spectroscopic studies, *RSC Adv.*, 2023, **13**, 32185–32198.
82 S. Gamsey, A. Miller, M. M. Olmstead, C. M. Beavers, L. C. Hirayama, S. Pradhan, R. A. Wessling and B. Singaram, Boronic acid-based bipyridinium salts as tunable receptors for monosaccharides and α-hydroxycarboxylates, *J. Am. Chem. Soc.*, 2007, **129**, 1278–1286.
83 X. T. Zhang, S. Wang and G. W. Xing, Novel Boronlectins Based on Bispyridium Salt with a Flexible Linker: Discriminative Sensing of Lactose and Other Monosaccharides and Disaccharides in Aqueous Solution, *Chem. – Asian J.*, 2015, **10**, 2594–2598.
84 C. Schmuck and M. Schwegmann, A naked-eye sensing ensemble for the selective detection of citrate-but not tartrate or malate- in water based on a tris-cationic receptor, *Org. Biomol. Chem.*, 2006, **4**, 836.
85 R. V. Velázquez-Castillo, M. K. Salomón-Flores, A. O. Viviano-Posadas, I. J. Bazany-Rodríguez, C. Bustos-Brito, J. M. Bautista-Renedo, N. González-Rivas, L. D. Rosales-Vázquez and A. Dorazco-González, Recognition and visual detection of ADP and ATP based on a dinuclear Zn(II)-complex with pyrocatechol violet in water, *Dyes Pigm.*, 2021, **196**, 109827.
86 G. Springsteen and B. Wang, Alizarin Red S. as a general optical reporter for studying the binding of boronic acids with carbohydrates, *Chem. Commun.*, 2001, **17**, 1608–1609.
87 I. Y. Zhang, J. Wu and X. Xu, Extending the reliability and applicability of B3LYP, *Chem. Commun.*, 2010, **46**, 3057–3070.
88 F. Weigend and R. Ahlrichs, Balanced basis sets of split valence, triple zeta valence and quadruple zeta valence quality for H to Rn: Design and assessment of accuracy, *Phys. Chem. Chem. Phys.*, 2005, **7**, 3297–3305.
89 Y. Takano and K. N. Houk, Benchmarking the conductor-like polarizable continuum model (CPCM) for aqueous solvation free energies of neutral and ionic organic molecules, *J. Chem. Theory Comput.*, 2005, **1**, 70–77.
90 J. Contreras-García, R. A. Boto, F. Izquierdo-Ruiz, I. Reva, T. Woller and M. Alonso, A benchmark for the non-covalent interaction (NCI) index or··· is it really all in the geometry?, *Theor. Chem. Acc.*, 2016, **135**, 1–14.
91 R. F. W. Bader, Atoms in Molecules, *Acc. Chem. Res.*, 1985, **18**, 9–15.
92 *Bruker SAINT and SADABS*, Bruker AXS Inc., Madison, Wisconsin, USA, 2007.
93 G. M. Sheldrick, A short history of SHELX, *Acta Crystallogr., Sect. A: Found. Crystallogr.*, 2007, **64**, 112–122.
94 C. B. Hübschle, G. M. Sheldrick and B. Dittrich, ShelXle: A Qt graphical user interface for SHELXL, *J. Appl. Crystallogr.*, 2011, **44**, 1281–1284.

